Dryden Lectureship in Research

# Some Aspects of Shock-Wave Research

## I. I. Glass

*University of Toronto Institute for Aerospace Studies, Toronto, Ontario, Canada*

## Nomenclature

| | |
|---|---|
| $a$ | = speed of sound |
| $C$ | = wedge corner |
| CMR | = complex-Mach reflection |
| DMR | = double-Mach reflection |
| $e$ | = specific internal energy |
| $E$ | = total specific energy, $\frac{1}{2}(u^2 + v^2) + e$ |
| $h$ | = flow enthalpy |
| $\bar{H}$ | = pseudostationary total enthalpy, $= \frac{1}{2}(\bar{u}^2 + \bar{v}^2) + h$ |
| $I$ | = incident shock wave in shock tube |
| $K$ | = kink in CMR reflected wave $R$ |
| $M, M'$ | = first and second Mach stems in DMR |
| $\bar{M}^2$ | = self-similar Mach number $(\bar{M})$, $= (\bar{u}^2 + \bar{v}^2)/a^2$ |
| MR | = Mach reflection (SMR, CMR, DMR, TDMR) |
| $M_s$ | = incident shock wave $(I)$ Mach number |
| $p$ | = static pressure |
| $P$ | = reflection point; point where RR $\leftrightarrow$ CMR and CRM $\leftrightarrow$ DMR lines meet |
| $R$ | = gas constant |
| $R, R'$ | = first and second reflected shock waves in DMR |
| RR | = regular reflection |
| $S, S'$ | = first and second slipstreams in DMR |
| SMR | = single-Mach reflection |
| $t$ | = time |
| $T$ | = temperature |
| TDMR | = terminal double-Mach reflection, where $\chi' = 0$ |
| $T, T'$ | = first and second triple points in DMR |
| $u$ | = $(u, v)$ velocity field |
| $\bar{u}$ | = $u - \xi$ pseudostationary velocity component in the $x$ direction |
| $\bar{v}$ | = $v - \eta$ pseudostationary velocity component in the $y$ direction |
| $u, v$ | = velocity components in the $x$ and $y$ directions |
| $x, y$ | = Cartesian coordinates |
| $\alpha$ | = velocity-deflection angle in slipstream shear layer |
| $\gamma$ | = specific heat ratio |
| $\delta$ | = angle between incident $(I)$ and reflected $(R)$ shock waves |
| $\delta^*$ | = boundary-layer displacement thickness |
| $\epsilon$ | = Mach-stem curvature angle |
| $\eta$ | = $(y - y_0)/(t - t_0)$ pseudostationary coordinate |
| $\theta_d$ | = boundary-layer displacement effect on the difference in the flow angles of the incident and reflected shock waves |
| $\theta_{2m}$ | = flow detachment angle |
| $\theta_w$ | = wedge angle |
| $\theta_w'$ | = effective wedge angle, $= \theta_w + \chi$ |
| $\xi$ | = pseudostationary coordinate, $= (x - x_0)/(t - t_0)$ |
| $\rho$ | = flow density |
| $\phi$ | = wave angle |
| $\chi, \chi'$ | = first and second triple-point trajectory angles |

## Introduction

SHOCK-WAVE phenomena on Earth[1-3] are common and important occurrences in our lives. For example, we hear them from the cradle to the grave as terrorizingly crashing or rumbling thunder following lightning discharges.[4-7] It is estimated that 1000 thunderstorms occur on Earth at any moment. In the primordial state of our Earth, such shock waves are credited as being enormously more efficient in creating the building and replicating blocks of life, such as ATP, RTP, and DNA,[2,8] than the radiation from the sun. Yet, paradoxically enough, all life is threatened today by the radiation and the very shock waves that might be unleashed by a thermonuclear war.[9-11]

The lethal overpressures and winds induced by shock waves are now well understood,[12,13] even though our eyes cannot see the shock waves generated by lightning, firearms, or explosions in air, since air is a transparent gas. Special optical methods (interferometry, schlieren, and shadow photography) must be used to make shock waves visible.[14] The more intense the explosion or rapidity and size of energy release, the higher is the velocity of the resulting shock wave, and its attendant increases in pressure, density, and flow velocity, and the greater is the possible devastation. The shock wave becomes less destructive with time or distance as it compresses and heats the enveloped air, thereby dissipating its energy, until it becomes a harmless sound wave.[12-14]

At sea level, where the mean free path is small ($6.6 \times 10^{-6}$ cm), the thickness of the shock front is about tenfold this value. Consequently, it is quite incredible how rapidly the shock wave changes from its quiescent ambient conditions in

I. I. Glass obtained his bachelor's and master's degrees in engineering physics-aeronautical engineering, and his doctorate degree in aerophysics at the University of Toronto in 1950, when he joined UTIAS. His fields of study have centered on gasdynamics and shock-wave phenomena. Currently, he is interested in various types of nonstationary oblique-shock-wave reflections in perfect, imperfect, and dusty gases; implosion dynamics with a view to producing new materials; nonstationary laminar boundary layers behind dusty-gas shock waves. He has lectured and published widely, and his two books — *Shock Tubes* (with Professor J. G. Hall) and *Shock Waves and Man* — have been sought after for many years. The latter has been translated into Russian, Polish, Hindi, Chinese, and Japanese. Professor Glass is a Fellow of the Royal Society of Canada, the American Physical Society, the American Institute of Aeronautics and Astronautics, the American Association for the Advancement of Science, and the Canadian Aeronautics and Space Institute. He received the highest honor that the University of Toronto can bestow on one of its faculty members being named a distinguished "University Professor" in October 1981. In 1985, he was awarded an "Honorary Professorship" by the Nanjing Aeronautical Institute, Nanjing, China. He is the first foreign visitor to receive this top academic honor.

front, to one of destruction behind it through molecular collisions. In outer space, where the mean free path is very large, the shock thickness can be thousands of kilometers, and the various changes through it are much more gradual.

Aside from the lightning-thunder process, shock waves on Earth are also generated by intense volcanic eruptions and meteor impact. The recent eruption of Washington's Mt. St. Helens is estimated to have had an energy release equivalent to 50 Mtons of TNT or about 3000 bombs of the type used to destroy Hiroshima. The eruption of the Krakatoa volcano in 1883 in Indonesia is estimated to have had an energy release of 5000 Mtons of TNT or 100 times as powerful as Mt. St. Helens. Perhaps the greatest eruption in recorded history occurred in Tambora, Indonesia, in 1815, with an energy release of about tenfold that of Krakatoa. The airborne ash caused "a year without a summer" in 1816 and 12,000 people were killed.[15]

If a meteor of the size that produced the Arizona Crater ever impacted in a big city, it could be as devastating as a multimegaton bomb.[16] An energy release equivalent to 15 Mtons TNT is estimated to have been released on impact over 50,000 years ago. Yet, there is geological evidence of craters formed millions of years ago from an energy release of 50 million Mtons of TNT, caused by asteroid impact. Such asteroids orbit the sun between Mars and Jupiter. A few orbit the sun to pass inside the orbit of the Earth. However, not all are known. It is estimated that perhaps 800 ± 300 such Apollo asteroids, larger than 1 km, may remain undetected. An impact would release an energy of about 100,000 Mtons of TNT and leave a crater 20 km wide. As a matter of fact, a news item [Washington (Reuter) 14.2.81] reports that NASA urged the U.S. government to organize "Project Spacewatch" to keep track of such asteroids and meteors and, if necessary, to send spacecraft armed with hydrogen bombs to deflect those that may menace to impact the Earth.

Yet, we need not associate shock waves only with destruction. Our modern industrial society could not have been built without the use of explosives that produce shock waves. Explosives are used in building highways, canals, tunnels, harbors, railroads, and subways; in mining, agriculture, engineering; and in the space programs for precise timing, activating, and cutting requirements.[1] Recently, shock waves produced by a high-voltage discharge or 5–10 mg of lead azide ($PbN_6$) have been applied successfully to medicine in the breaking up of large kidney stones and bladder stones to relieve suffering and possibly death.[17,18] More recently, lasers have been used as an energy source for the same purpose with some promising results.[19] It is estimated that 50,000 successful operations have been performed using the spark-discharge machine described in Ref. 17, which is quite expensive. The cost factor (several million dollars) is important for use in the Third World, where the occurrence of such stones are more common. It partly motivated the work in Refs. 18 and 19 to reduce costs by a factor of 10, at least. Basically, the three systems are similar in that the energy discharge (spark, explosive, laser) takes place at the focus of an ellipsoidal mirror and is refocused at the second focus located on the kidney stone, as a powerful implosion wave, which breaks up the obstructing stone. It may take many shots to break up a stone. In the case of bladder stones, the explosive is used directly against the stone.

In space, the best example of shock-wave phenomena is the magnetosphere[1] flow about planets in our solar system. Our Earth is an excellent example. It becomes a spherical-flow model in a solar wind at hypersonic speeds ($M \sim 13$). The solar wind is composed of ionized hydrogen, helium, some other heavier nucleons and electrons. This plasma is electrically neutral. It blows with a supersonic velocity of 400 km/s with a bulk number density of about 10 particles/$cm^3$ having an average kinetic temperature of about $10^5$ K. The interaction of the ionized particles with the Earth's dipole magnetic field distorts it into a streamlined shape with the magnetopause as a boundary, that is, where the ionized gas can no longer

penetrate the Earth's magnetic field. The collisionless bow shock in front of the line of symmetry is about 30 Earth radii from the Earth's center. The stagnation point on the magnetopause is about 20 Earth radii from the Earth's center on this line. The standoff distance of the bow shock from the stagnation point is about 10 Earth radii (about 64,000 km). The bow shock itself is many thousands of kilometers thick. The subsonic plasma behind the bow shock probably has a tenfold increase in temperature to about $10^6$ K. Near the Earth the magnetopause cavity contains the famous Van Allen radiation belts. The magnetopause cavity resembles a comet, and the tail may extend several million kilometers downwind.

Similar flows can exist around a star. A recent relevant study of this phenomenon is given in Ref. 20. Of the many shock-wave phenomena in space, one of the most interesting is the existence of shock waves in the spiral arms of galaxies[21] such as our own Milky Way. Densities can increase by about an order of magnitude, making possible the birth of young blue stars.

## Pseudostationary Oblique Shock-Wave Reflections

This problem was first investigated by E. Mach in 1878,[22] and has since occupied many scientists and engineers, and where my students and I have made some worthwhile contributions over the past decade. The problem is known as "pseudostationary oblique shock-wave reflections." Although much more is known about this problem now than when Mach started it all, there is still a great deal to learn. It is of interest for two main reasons: first, the problem involves a great deal of gasdynamics of perfect and imperfect flows (frozen and equilibrium, inviscid and viscous); second, our experimental (interferometric) shock-tube data have provided computational fluid dynamicists, who are working on explosion dynamics, with the means of checking their numerical simulations for accuracy. The latter data provide engineers with pressure, velocity, and other flow properties required to build explosion-resistant structures. To date, such simulations have proved to be extremely good, considering that the numerical solutions solve only the inviscid Euler equations, whereas the experimental data come from flows that are viscous and can have real-gas effects as well.

### Analysis

Unlike linear waves encountered in acoustics and light, shock waves are nonlinear. For example, the reflected wave angle is different from the angle of incidence, and the physical quantities across shock waves such as pressure, density, temperature, and flow velocity are highly nonlinear. The simplest method of studying pseudostationary oblique shock-wave reflections is in a shock tube. Here a planar shock wave $M_s$ collides with a sharp compressive wedge of fixed angle $\theta_w$, and gives rise to regular reflection (RR) and three types of Mach reflections (MR) — namely, single- (SMR), complex- (CMR), and double-Mach reflection (DMR) — as shown in Figs. 1 and 2. (The various symbols are defined on the figures.) It is seen that RR consists of two shock waves meeting at the reflection point $P$. However, MR consists of three shock waves meeting at the triple point $T$. It has been shown[23-25] that such flows are self-similar, i.e., they look the same with time except for an increased scale. Consequently, the Mach stem grows with time (or distance) along the triple-point trajectory angle $\chi$. It may also be mentioned that this angle represents an effective wall for the incident shock wave $I$ to reflect from and produce a reflected shock wave $R$. This provides the subsequent use of the effective wedge angle $\theta'_w = \theta_w + \chi$ as a useful parameter.

It is seen that regular reflection consists of an incident shock wave $I$ and a reflected shock wave $R$, which may be attached at the wedge corner $C$, or detached from it. The standoff distance $s$, divided by the distance $L$, which the incident shock wave $I$ has traveled from the corner, remains constant. The

Fig. 1 Types of oblique shock-wave reflections in pseudostationary flow. a) RR and b) SMR. *I*, incident shock wave; *R*, reflected shock wave; $M_s$, incident shock-wave Mach number; $\theta_w$, wedge angle; *C*, wedge corner; (0), initial state; (1), (2), (3), subsequent states; $\phi$, wave angle; $\theta$, flow angle; $\delta$, angle between *I* and *R*; $\omega'$, angle between *R* and wall in RR, and between *R* and $\chi$ in MR; $\chi$, triple-point; trajectory angle; T', triple point; *M*, Mach stem; *S*, slipstream; $\theta'_w = \theta_w + \chi$, effective wedge angle in MR. c) CMR and d) DMR. *K*, kink; $\ell$, distance between *K* and *C*; T', second triple point; M', second Mach shock; *R*, straight reflected shock wave; R', curved reflected shock wave; S', second slipstream; $\chi'$, second triple-point trajectory angle; *s*, standoff distance; *L*, distance traveled by *I* from corner *C*.

Fig. 2 Types of double-Mach reflections in pseudostationary flow. a) T' lies about $\chi$, b) T' lies along $\chi$, c) T' lies below $\chi$, d) terminal double-Mach reflection (TDMR) where T' lies along wedge surface, M' has vanished, and R' is a regular reflection.

reflected shock wave is curved if the flow behind it is subsonic, and it may have a straight portion near the reflection point if the flow there is supersonic and uniform (see Figs. 1a and 1c).

Mach reflection (Figs. 1b-1d), on the other hand, consists of incident *I* and reflected *R* shock waves, a Mach stem *M*, and a slipstream *S*. The three shocks meet at the triple point T, and the slipstream *S* separates states (2) and (3), even though they have the same pressure and flow inclination. SMR has a curved reflected wave. CMR has a kink in the reflected wave, which is caused by an interacting compression wave. In DMR, the kink becomes sharp and a second Mach shock M' is formed that finally extends to the slipstream *S*. As a result, a second triple point T' and a second slipstream S' are also formed. In this case, the reflected portion *R* is straight and the

flow behind it is supersonic. The reflected shock *R* in SMR and R' in all other Mach-reflection (MR) cases can also be attached or detached (see Figs. 1b-1d and 2b-2d).

The question arises, given the initial conditions of the gas $p_0$, $T_0$, $\gamma$, the shock Mach number $M_s$, and the wedge angle $\theta_w$, can one predict the resulting reflection a priori? The answer is "yes." This can be obtained from the following analysis.

It has been noted previously that such two-dimensional wedge flows are self-similar. Consequently, instead of three independent variables *x*, *y*, and *t*, the reflection phenomenon can be described in terms of two independent variables $x/t$ and $y/t$. The reflection point P, in regular reflection, and the triple point T, in Mach reflection, are chosen as specific points mov-

ing at constant velocity with respect to the wedge corner $C$. By attaching frames of reference to these points, the reflections become pseudosteady (Fig. 1). Consequently, the steady-flow equations of motion can be applied to each shock wave in turn, such that

Continuity:

$$\rho_i u_i = \rho_j u_j \sin(\phi_i - \theta_j) \qquad (1)$$

Tangential momentum:

$$\rho_i \tan\phi_i = \rho_j \tan(\phi_j - \theta_j) \qquad (2)$$

Normal momentum:

$$p_i + \rho_i u_i^2 \sin^2\phi_i = p_j + \rho_j u_j^2 \sin^2(\phi_i - \theta_j) \qquad (3)$$

Energy:

$$h_i + \tfrac{1}{2} u_1^2 \sin^2\phi_i = h_j + \tfrac{1}{2} u_j^2 \sin^2(\phi_i - \theta_j) \qquad (4)$$

where $\rho_i$ is the flow density of the initial state in front of the shock wave and $\rho_j$ is the flow density in the final state behind the shock wave, the same for the flow velocity $u$, pressure $p$, specific flow enthalpy $h$, wave angle $\phi$, and flow-deflection angle $\theta$. An equation of state

$$p = \rho R T \qquad (5)$$

is also used for a perfect gas or $p = p(\rho, T)$ for an imperfect gas. In addition, the boundary condition for regular reflection must be used so that the flow is parallel to the wedge surface (Fig. 1)

$$\theta_1 = \theta_2 \qquad (6)$$

For Mach reflection, across the contact surface or slipstream, the pressure must be continuous

$$p_2 = p_3 \qquad (7)$$

and the flow deflections must also be continuous or

$$\theta_3 = \theta_1 - \theta_2 \qquad (8)$$

It has been shown by von Neumann[26,27] and verified by many experimentalists that in pseudostationary flow a regular reflection will undergo transition to a Mach reflection when $\theta_2 = \theta_{2m}$, that is, when the wedge angle $\theta_w$ produces the max-

imum possible flow deflection $\theta_{2m}$. This angle is also known as the flow-detachment angle. For further details, see Refs. 14 and 26-28.

As noted previously, Mach reflection (Fig. 1) can, in turn, be divided into SMR, CMR, and DMR; and DMR can be subdivided into four subtypes (Fig. 2), depending on whether or not the second triple-point trajectory angle $\chi'$ is above, equal to, or below the first triple-point trajectory angle $\chi$. Finally, there is the terminal double-Mach reflection (TDMR) case, where $\chi' = 0$. That is, the second triple point lies on the wedge surface. The second Mach shock disappears and the reflected shock wave reflects as a regular reflection. Such reflections occur readily in gases with low values of $\gamma$, such as Freon-12[25] or SF$_6$.[28] They are not possible in perfect monatomic, diatomic, or triatomic gases, although they are possible when these gases are imperfect and have a low effective $\gamma$ (see Fig. 2d).

It is assumed that SMR becomes a CMR when the flow with respect to the first triple point T becomes sonic, i.e., $M_{2T} = 1$. This assumption is based on experimental observation and computational simulation.[29-35] The same heuristic approach is taken for CMR↔DMR transition, and the condition is applied to the kink or second triple point K or T' or $M_{2K} = 1$. A change of curvature occurs in the reflected wave $R$, which steepens into a sharp second triple point T'. This marks the formation of the second Mach shock $M'$, and a straight reflected shock $R$, before $M'$, and a curved reflected shock $R'$, after $M'$. The flow behind $R$ is supersonic. It should be noted that $M'$ grows in strength and length until it comes close to the slipstream $S$. Ideally, it should terminate there. Then it raises the problem: How can the contact front remain stable with a sharp pressure gradient applied to it? Interferometrically, the Mach shock appears to go around the rolled-up slipstream; in this case, as a compression wave.[36-39] This is also verified by numerical simulation of the interferograms in question for DMR in different gases.[33,34]

If the preceding equations and conditions are applied and solved, it is possible to obtain a plot in the $(M_s, \theta_w, \text{or } \theta_w')$ plane,[28] delineating the various regions of RR, SMR, CMR, and DMR and their transition lines, as shown in Figs. 3 and 4, for example, for perfect and imperfect air in vibrational, dissociational, and ionizational equilibrium, over a very large initial shock Mach number range $1 < M_s < 20$. It can be seen that, for $M_s > 10$, the curves do not change for perfect air,[40] but undulate for equilibrium air as new degrees of freedom are excited.

By assuming that the Mach stem is straight and perpendicular to the wedge surface, from the triple point T, it is possible to obtain an expression for the triple-point trajectory angle $\chi$,[41] as well as the second triple-point trajectory angle $\chi'$.[42] Unfortunately, the Mach stem is usually curved. It is
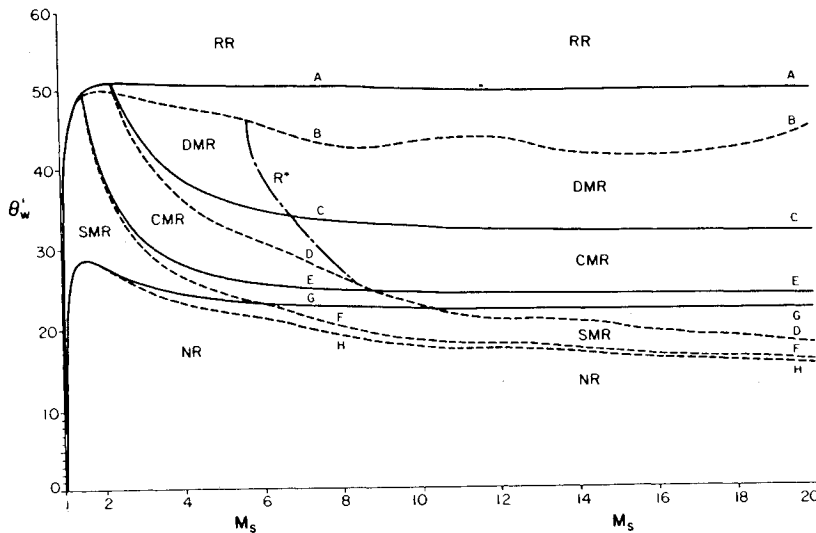


Fig. 3   Regions of various types of shock-wave reflection in $(M_s, \theta_w)$ plane. Solid lines are for perfect air with $\gamma = 1.40$; dashed lines are for imperfect air at $P_0 = 15$ Torr and $T_0 = 300$ K. Line $R^*$ shows where $\omega'$ is $(+)$, $\chi' > \chi$ in DMR (left), and $\omega'$ is $(-)$ or $\chi' < \chi$ in DMR (right). On the line $R^*$, $\chi' = \chi$.
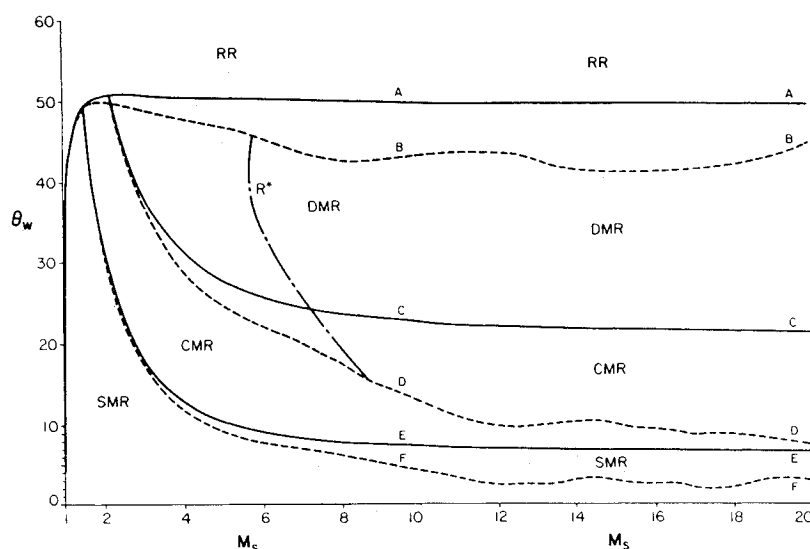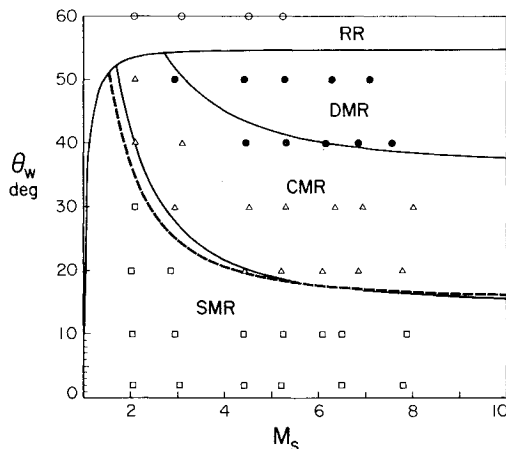
Fig. 4   Regions of various types of shock-wave reflection in $(M_s, \theta'_w)$ plane. Solid lines are for perfect air with $\gamma = 1.40$; dashed lines are for imperfect air at $P_0 = 15$ Torr and $T_0 = 300$ K. Line $R^*$ shows where $\omega'$ is $(+)$, $\chi' > \chi$ in DMR (left), and $\omega'$ is $(-)$ or $\chi' < \chi$ in DMR (right). On the line $R^*$, $\chi' = \chi$.



Fig. 5a   Regions and transition lines of regular (RR) and Mach (MR) reflections in the $(M_s, \theta_w)$ plane for frozen argon $(\gamma = 5/3)$ and experimental data. For SMR $\leftrightarrow$ CMR transition boundary, solid line represents $M_{2T} = 1$ and dashed line represents $\delta = 90$ deg. Experimental data: o RR, □ SMR, △ CMR, ● DMR (Ref. 31).
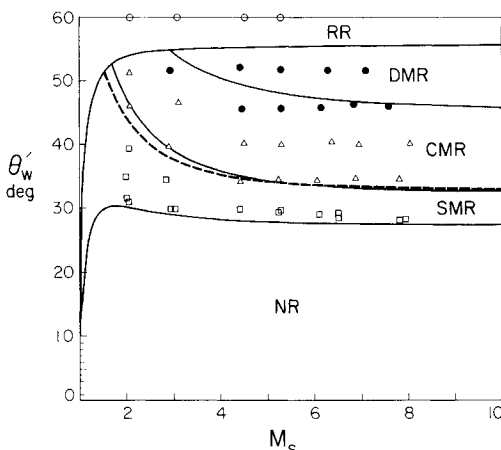


Fig. 5b   Regions and transition lines of regular (RR) and Mach (MR) reflections in the $(M_s, \theta'_w)$ plane for frozen argon $(\gamma = 5/3)$ and experimental data. For SMR $\leftrightarrow$ CMR transition boundary, solid line represents $M_{2T} = 1$ and dashed line represents $\delta = 90$ deg. Experimental data: o RR, □ SMR, △ CMR, ● DMR (Ref. 31).

concave at the lower shock Mach number $M_s$, for significant stem heights, and convex[43] at higher Mach numbers. This introduces an error in determining $\chi$ and $\chi'$, especially when $\chi$ is small.[43]

### Comparison with Experimental Results in the $M_s$, $\theta_w$, or $\theta'_w$ Plane

The interferometric, schlieren, and shadowgram data from the Institute for Aerospace Studies were obtained in the $10 \times 18$-cm Hypervelocity Shock Tube. The major instrument for this purpose was a 23-cm-diam field-of-view Mach-Zehnder interferometer with a giant-pulse Q-switched ruby laser with a frequency doubler at 6943 and 3471.5 Å, having an exposure time of 15 ns. The latter was short enough to photograph the strongest shock wave without blurring.

Figures 5-9 show comparisons of the analytical domains and transition boundaries for RR, SMR, CMR, and DMR with experiments in argon,[31] oxygen,[41] nitrogen,[30] air,[36] carbon dioxide,[37] and sulfurhexafluoride.[38] In addition, the detailed results obtained by Ikui et al.[25] for air, $CO_2$, and Freon-12 are shown and discussed.

An examination of Fig. 5a shows the experimental results for RR and MR in Ar on an $(M_s, \theta_w)$ plane. In our early experiments, the major effort was to show that the various regimes were predictable from the foregoing analysis. As more experience was gathered, it become clear that the various transition lines were the sensitive lines to be tested. Consequently, the various analytical regimes look reasonably well validated. Three DMR runs (1 at 50 deg and 2 at 40 deg) lie in the CMR regime. All of the other experiments are in their appropriate regimes. It has been found[43] that, along with $M_{2T} = 1$ for SMR $\leftrightarrow$ CMR, another condition that must be satisfied is $\delta > 90$ deg. On all graphs, the dashed line represents $\delta = 90$ deg and its lower branch lies above the solid line for SMR $\leftrightarrow$ CMR, where $M_{2T} = 1$. The upper branch of the dashed line lies below the shock line, where $M_{2T} \neq 1$, yet. It can be seen that two points at $\theta_w = 40$ and 20 deg are improved to lie in CMR.

When these results are plotted on an $(M_s, \theta'_w)$ plane (Fig. 5b), which is more accurate since a relation for $\chi$ is not required, paradoxically, a poorer agreement is obtained for Ar. Now four DMR runs, one at $\theta_w = 50$ deg and three at $\theta_w \sim 45$ deg, definitely lie in the CMR regime and two other CMR's are borderline runs; one CMR run lies in the SMR regime at $M_s \sim 4$, all other runs are in their appropriate regimes. Since no runs were made along the RR $\rightarrow$ MR transition line, little can be said about the "von Neumann paradox" (where RR persists into the MR regime) or possible boundary-layer effects. No real-gas effects occur in Ar for the pressures and
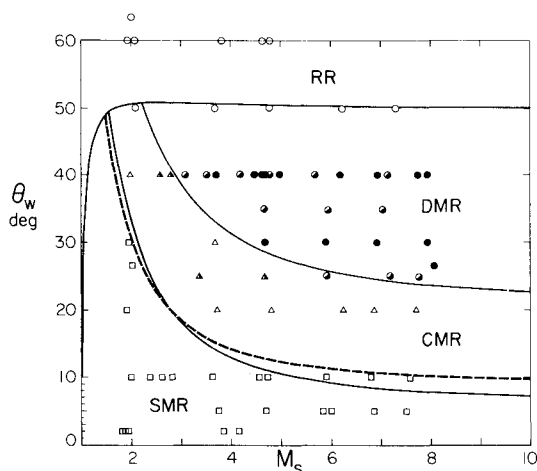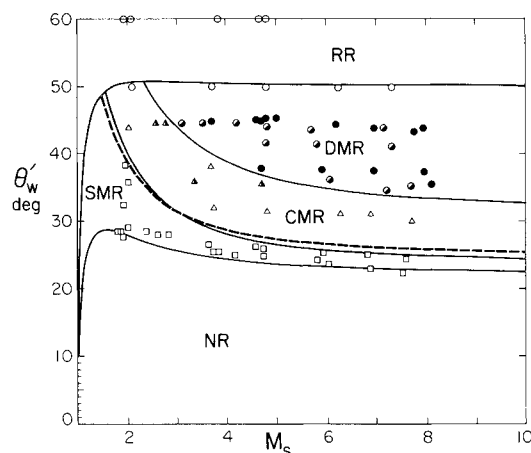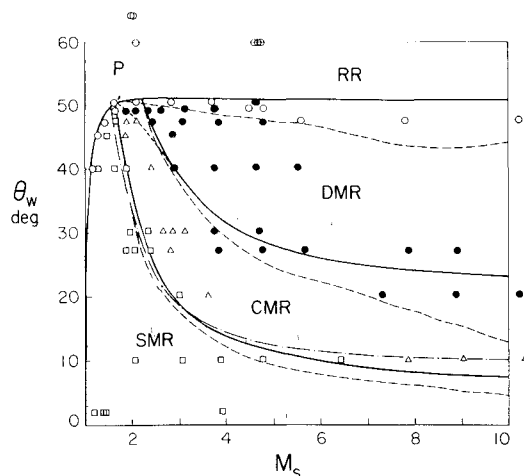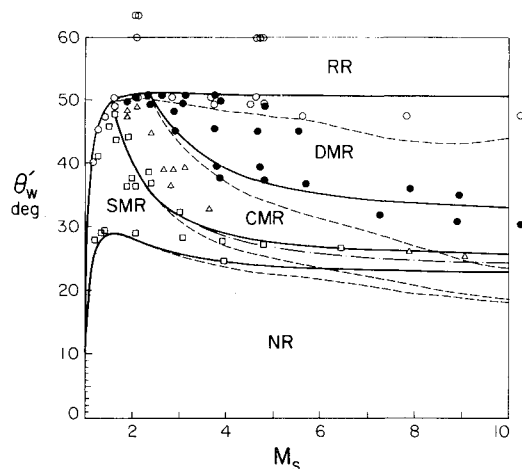
Fig. 6a   Regions and transition lines of regular (RR) and Mach (MR) reflections in the $(M_s,\theta_w)$ plane for frozen $N_2$ and $O_2$ ($\gamma = 7/5$) and experimental data. For SMR↔CMR transition boundary, solid line represents $M_{2T} = 1$ and dashed line represents $\delta = 90$ deg. Experimental data: o RR, □ SMR, △ CMR, ● DMR ($N_2$—Ref. 30); ◨ SMR, △ CMR, ◐ DMR ($O_2$—Ref. 41).



Fig. 6b   Regions and transition lines of regular (RR) and Mach (MR) reflections in the $(M_s,\theta_w')$ plane for frozen $N_2$ and $O_2$ ($\gamma = 7/5$) and experimental data. For SMR↔CMR transition boundary, solid line represents $M_{2T} = 1$ and dashed line represents $\delta = 90$ deg. Experimental data: o RR, □ SMR, △ CMR, ● DMR ($N_2$—Ref. 30); ◨ SMR, △ CMR, ◐ DMR ($O_2$—Ref. 41). NR is the no-reflection region.



Fig. 6c   Regions and transition lines of regular (RR) and Mach (MR) reflections in the $(M_s,\theta_w)$ plane for air and experimental data. Solid lines are for air as a perfect gas ($\gamma = 7/5$). For SMR↔CMR transition boundary, solid line represents $M_{2T} = 1$ and dash-dot line represents $\delta = 90$ deg. Dashed lines are for imperfect air at $P_0 = 15$ Torr and $T_0 = 300$ K. Experimental data: o RR, □ SMR, △ CMR, ● DMR (Ref. 36).



Fig. 6d   Regions and transition lines of regular (RR) and Mach (MR) reflections in the $(M_s,\theta_w')$ plane for air and experimental data. Solid lines are for perfect air ($\gamma = 7/5$). Dashed lines are for imperfect air at $P_0 = 15$ Torr and $T_0 = 300$ K. For SMR↔CMR transition boundary, solid line represents $M_{2T} = 1$ and dashed line represents $\delta = 90$ deg. Experimental data: o RR, □ SMR, △ CMR, ● DMR (Ref. 36). NR is the no-reflection region.
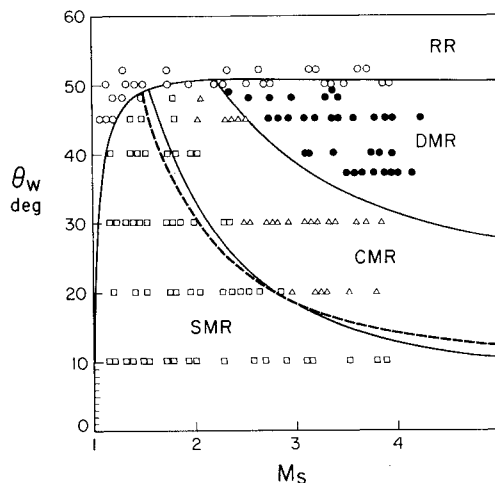


Fig. 6e   Regions and transition lines of regular (RR) and Mach (MR) reflections in the $(M_s,\theta_w)$ plane for perfect air ($\gamma = 7/5$) and experimental data. For SMR↔CMR transition boundary, solid line represents $M_{2T} = 1$ and dashed line represents $\delta = 90$ deg. Experimental data: o RR, □ SMR, △ CMR, ● DMR (Ref. 25).

Mach numbers of these experiments, as the relaxation lengths are too large and the gas remains frozen with a $\gamma = 5/3$.

Figures 6a and 6b show the results of $N_2$ and $O_2$ in the $(M_s, \theta_w)$ and $(M_s,\theta_w')$ planes. In Fig. 6a, the six RR runs at the RR→MR transition are only marginally below it. All runs except a DMR at $M_s = 6$ lie in their appropriate regimes. The line for $\delta = 90$ deg is very helpful in this case, because all of the SMR runs lie in their appropriate regimes. The same comments apply to Fig. 6b. It is seen that as $\gamma$ decreases the NR and SMR→CMR lines lie closer together, preventing a clear-cut distinction of the experiments.

Figures 6c and 6d show the results for air on the $(M_s,\theta_w)$ and $(M_s,\theta_w')$ planes.[36] It is seen from Fig. 6c that at the RR↔MR transition line two RR runs lie in the SMR regime; one RR run lies in the CMR regime and seven RR runs lie in the DMR regime. This definitely shows the persistence of RR into the MR regime. Subsequently, it will be shown that this is due to the shock-induced boundary layer on the wedge surface. It is also known that the CMR↔DMR line must curve and meet the SMR→CMR line at point P on the RR↔MR line, as the
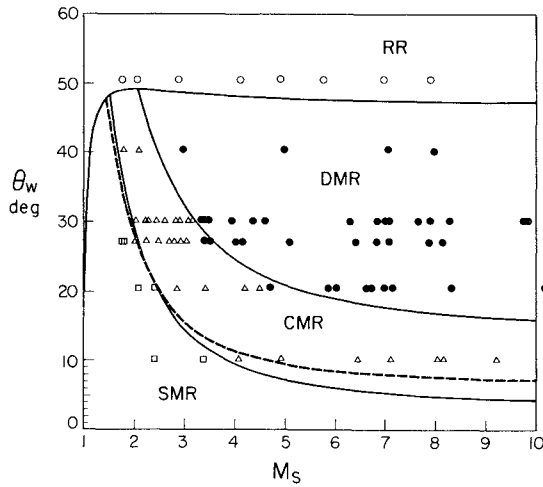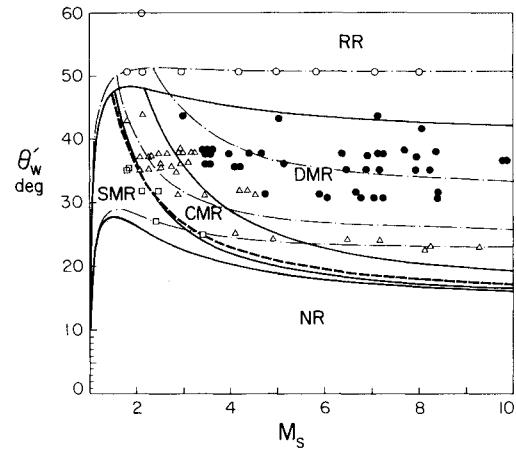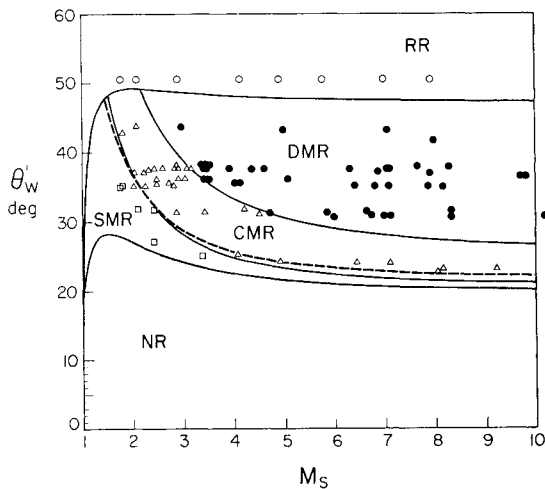
Fig. 7a Regions and transition lines of regular (RR) and Mach (MR) reflections in the $(M_s, \theta_w)$ plane for $CO_2$ as a perfect gas $(\gamma = 1.29)$ and experimental data. For SMR↔CMR transition boundary, solid line represents $M_{2T} = 1$ and dashed line represents $\delta = 90$ deg. Experimental data: o RR, □ SMR, △ CMR, ● DMR (Ref. 37).


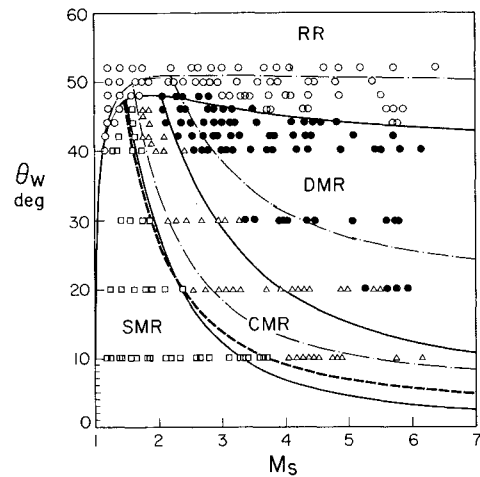
Fig. 7d Regions and transition lines of regular (RR) and Mach (MR) reflections in the $(M_s, \theta'_w)$ plane for vibrational equilibrium $CO_2$ and experimental data. For SMR↔CMR transition boundary, solid line represents $M_{2T} = 1$ and dashed line represents $\delta = 90$ deg. Dash-dot lines are for frozen $CO_2$ $(\gamma = 7/5)$. Experimental data: o RR, □ SMR, △ CMR, ● DMR (Ref. 37). NR is the no-reflection region.



Fig. 7b Regions and transition lines of regular (RR) and Mach (MR) reflections in the $(M_s, \theta'_w)$ plane for $CO_2$ as a perfect gas $(\gamma = 1.29)$ and experimental data. For SMR↔CMR transition boundary, solid line represents $M_{2T} = 1$ and dashed line represents $\delta = 90$ deg. Experimental data: o RR, □ SMR, △ CMR, ● DMR (Ref. 37).
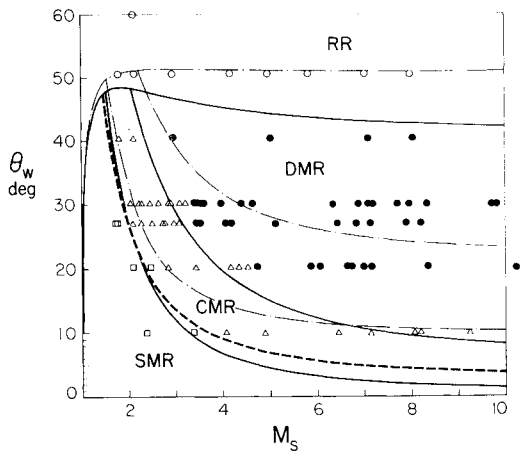


Fig. 7e Regions and transition lines of regular (RR) and Mach (MR) reflections in the $(M_s, \theta_w)$ plane for vibrational equilibrium $CO_2$ and experimental data. For SMR↔CMR transition boundary, solid line represents $M_{2T} = 1$ and dashed line represents $\delta = 90$ deg. Dash-dot lines are for frozen $CO_2$ $(\gamma = 7/5)$. Experimental data: o RR, □ SMR, △ CMR, ● DMR (Ref. 25).



Fig. 7c Regions and transition lines of regular (RR) and Mach (MR) reflections in the $(M_s, \theta_w)$ plane for vibrational equilibrium $CO_2$ and experimental data. For SMR↔CMR transition boundary, solid line represents $M_{2T} = 1$ and dashed line represents $\delta = 90$ deg. Dash-dot lines are for frozen $CO_2$ $(\gamma = 7/5)$. Experimental data: o RR, □ SMR, △ CMR, ● DMR (Ref. 37).
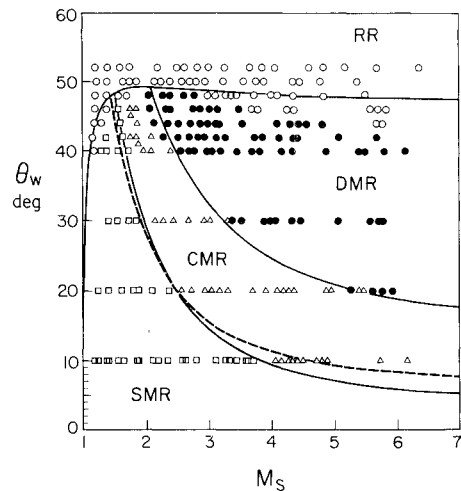


Fig. 7f Regions and transition lines of regular (RR) and Mach (MR) reflections in the $(M_s, \theta_w)$ plane for $CO_2$ as a perfect gas $(\gamma = 1.31)$ and experimental data. For SMR↔CMR transition boundary, solid line represents $M_{2T} = 1$ and dashed line represents $\delta = 90$ deg. Experimental data: o RR, □ SMR, △ CMR, ● DMR (Ref. 25).

distance between the two triple points TT' goes to zero there. As a consequence, the two DMR runs in CMR now lie in the appropriate regime. Real-gas effects shown by the equilibrium dashed lines do not explain the results, since the runs were done at different initial pressures. Eight DMR runs lie in the CMR regime and three SMR runs lie in the CMR regime. Consequently, it appears that better criteria are required for the RR→MR, SMR→CMR, and CMR→DMR transition lines. Similar remarks apply to Fig. 6d. Overall, the $\delta = 90$-deg line is not helpful in this case.

Figure 6e includes the detailed results of Ikui et al.[25] for air. It is seen that excellent agreement is obtained for RR at the RR→MR transition line. For $M_s > 2$, the runs lie marginally below it. One RR run lies in the SMR regime. Eight SMR's lie in the CMR regime. All CMR and DMR runs lie in their appropriate regimes. The perfect-gas ($\gamma = 7/5$) transition lines appear quite appropriate for their results. No significant evidence of the persistence of RR into MR regimes can be seen. The dashed line for $\delta = 90$ deg is not helpful in this case, but a new SMR→CMR line closer to the CMR→DMR line would place all of the SMR runs in their appropriate regime.

Figures 7a-7f deal with $CO_2$ in the $(M_s, \theta_w)$ or $(M_s, \theta'_w)$ plane. Figure 7a shows the experiments for transition lines based on a perfect gas, $\gamma = 1.29$. Although such lines are in error, since the vibrational relaxation lengths are short, and an equilibrium flow is appropriate, nevertheless, excellent agreement is obtained, by and large, for all points except two DMR's at $M_s \sim 3.5$ in the CMR regime and one at $M_s \sim 4.7$. One CMR at $M_s \sim 4$ agrees better with the $M_{2T} = 1$ criterion, and $\delta = 90$ deg is not helpful in this case. The regular reflection runs at $\theta_w = 50$ deg are not a test of the RR→MR transition, as they should have been done much closer to or below that line. Consequently, little can be said about boundary-layer effects in this case. Somewhat better agreement is obtained in the $(M_s, \theta'_w)$ plane shown in Fig. 7b.

The correct equilibrium transition is shown in Fig. 7c. Here, the frozen transition lines ($\gamma = 7/5$) are also shown for comparison. The agreement is quite good for the RR→MR line for the frozen case and poor for the rest of the frozen lines. Eight CMR runs lie in the equilibrium DMR regime and two SMR runs lie in the CMR region. In this particular case, the $\delta = 90$-deg line puts the SMR point at 10 deg in its proper place. It can be seen from Fig. 7a that the agreement there is accidentally better.

Figure 7d shows an $(M_s, \theta'_w)$ plot of the experimental runs in equilibrium $CO_2$. Although this is a more accurate plot, since $\chi$ does not have to be known, the results are poorer, since nine CMR's find themselves in the DMR region and one SMR occurs in the CMR regime. All of the DMR runs are located correctly, as well as all RR runs. Again, the various transition lines crowd together near $\theta_w = 20$ deg.

Figure 7e shows the detailed results of Ikui et al.[25] in the $(M_s, \theta_w)$ plane. It is clear that there is no agreement with $CO_2$ treated as a frozen gas ($\gamma = 7/5$). However, the vibrational equilibrium lines show very good agreement with the experiments over the entire Mach number range. Only two RR's lie below the RR→MR line in the SMR region. There are three DMR runs lying in the RR region above the RR→MR line. There is no evidence of RR persistence of viscous boundary-layer effects. Four SMR runs at $M_s = 2$ lie marginally in the CMR region; eleven CMR's lie in the DMR regime. Sometimes it is difficult to distinguish a CMR from a DMR, and perhaps this might account for some of the discrepancy. In this case, the $\delta = 90$-deg line makes it possible for several SMR runs at $\theta_w = 10$ deg to lie in their proper regime.

Figure 7f shows the results of Ikui et al.[25] plotted on the $(M_s, \theta_w)$ plane with their analytical lines for a perfect gas ($\gamma = 1.31$). It is seen that good agreement is obtained with all experimental runs by and large. The RR→MR line does not fit the results as well as for the equilibrium flow (Fig. 7e) since 14 RR runs lie in the DMR region. Only two RR runs lie in the SMR regime at $M_s \sim 1.5$ below the RR→MR line and two RR

in the CMR region. One borderline DMR run lies in the CMR regime at $\theta_w = 20$ deg. The $M_{2T} = 1$ line puts six CMR's in the proper regime, unlike $\delta = 90$ deg; the preceding results are analogous to those of Ando and Glass[37] (Fig. 7a).

Figure 8a shows the experimental results for Freon-12, from Ikui et al.[25] plotted on an $(M_s, \theta_w)$ plane, for their transition lines based on a perfect gas ($\nu = 1.141$). Again the perfect-gas lines give reasonable agreement. Four RR runs lie in the CMR region. Many DMR runs lie in the CMR regime. About four SMR's lie marginally in the CMR region and two CMR runs lie in the DMR regime. The dashed line is an experimental best fit for the RR→TDMR. Unfortunately, Ikui et al. did not extend the TDMR runs to higher $M_s$ and lower $\theta_w$ to provide a better picture of the TDMR regime, which can be predicted analytically (see Fig. 8b). Only in the CMR region is there evidence of the persistence of RR. An equilibrium $(M_s, \theta_w)$
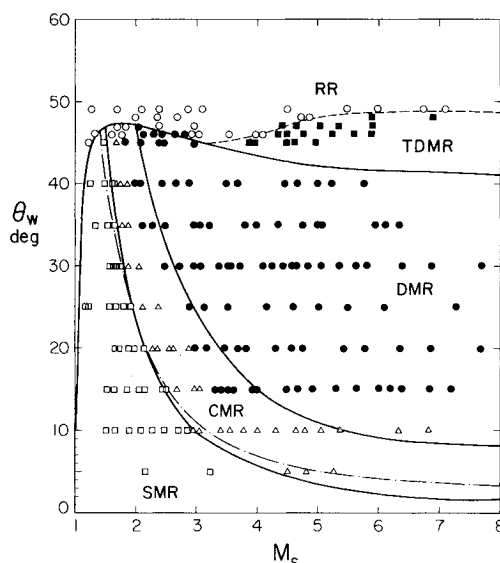


Fig. 8a    Regions and transition lines of regular (RR) and Mach (MR) reflections in the $(M_s, \theta_w)$ plane for Freon-12 as a perfect gas with $\gamma = 1.141$ and experimental data. Dashed line represents the experimental RR↔TDMR transition boundary. For SMR↔CMR, the solid line represents $M_{2T} = 1$, and the dash-dot line represents $\delta = 90$ deg. Experimental data: TDMR (terminal double-Mach reflection). ○ RR, □ SMR, △ CMR, ● DMR (Ref. 25).
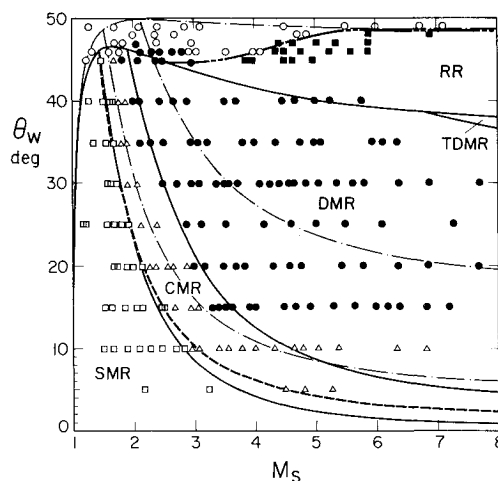


Fig. 8b    Regions and transition lines of regular (RR) and Mach (MR) reflections in the $(M_s, \theta_w)$ plane for Freon-12 and experimental data. Dash-dot lines represent the frozen flow ($\gamma = 4/3$). Solid lines represent equilibrium Freon-12. Dash-double dot line represents the RR↔TDMR experimental limit ■ TDMR (terminal double-Mach reflection). ○ RR, □ SMR, △ CMR, ● DMR (Ref. 25).

plot is shown in Fig. 8b. It also includes the transition lines for a frozen flow with $\gamma = 4/3$, for which the agreement with experiment is poor. This time, more DMR runs lie in the RR region including the TDMR runs. Note that the condition $\chi' = 0$ yields only a small TDMR region below the RR$\leftrightarrow$MR line. Consequently, one can only suspect that the detachment criterion of $\theta_2 = \theta_{2m}$ due to von Neumann is invalid for pseudostationary flow. The equilibrium SMR$\leftrightarrow$CMR is not improved from the one in Fig. 8a, nor does the criterion $\delta = 90$ deg help. The CMR$\leftrightarrow$DMR line does not improve overall the location of the runs. Some CMR runs are more poorly located and some DMR runs are better located in their respective regions.

Figures 9a and 9b show the results for SF$_6$ in the $(M_s,\theta_w)$ and $(M_s,\theta_w')$ planes.[38] Considerable effort was made in this case to check the transition lines themselves. Figure 9a shows the results for frozen $(\gamma = 4/3)$ and equilibrium flows. The frozen-flow lines do not represent the experiments. Two RR and two DMR runs lie in the CMR region below the RR$\rightarrow$MR transition lines. Six RR runs lie right on the RR$\rightarrow$MR transition line. There is no serious evidence of RR persistence up to $M_s \sim 6.5$ and two TDMR's at $M_s \sim 8$. One CMR run lies in the
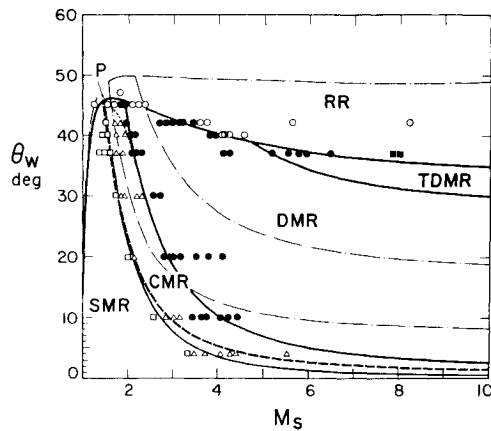
SMR region and five DMR's lie in the CMR regime. The $M_{2T} = 1$, rather than $\delta = 90$ deg, puts five CMR runs in their proper place. However, overall the agreement is good. Similar remarks can be made for the $(M_s,\theta_w')$ plot of Fig. 9b. Here, however, it is clear that DMR persists into the RR regime over the entire range of $M_s$. Consequently, the $(M_s,\theta_w')$ plot gives poorer rather than better agreement with the RR$\rightarrow$MR transition line. It should be noted that, if three-shock theory was used here rather than two, $\chi$ would have a value from 1 to 3 deg over the RR$\rightarrow$MR line, which would be pushed upward for better agreement with experiments than the present line. The small dashed line running from CMR$\rightarrow$DMR to point P on the RR$\rightarrow$MR transition line indicates the fact that in actuality this takes place. It makes for better agreement in Figs. 9a and 9b in that the DMR runs at $M_s \sim 2$ lie in their correct region. Again, the transition lines are too close, especially at $\theta_w \sim 10$ deg in Fig. 9b.

Figure 9c shows the SF$_6$ results in the $(M_s,\theta_w)$ plane for a perfect gas $(\gamma = 1.093)$. The experiments are quite well represented on this plot. Two RR runs lie below the RR$\leftrightarrow$MR
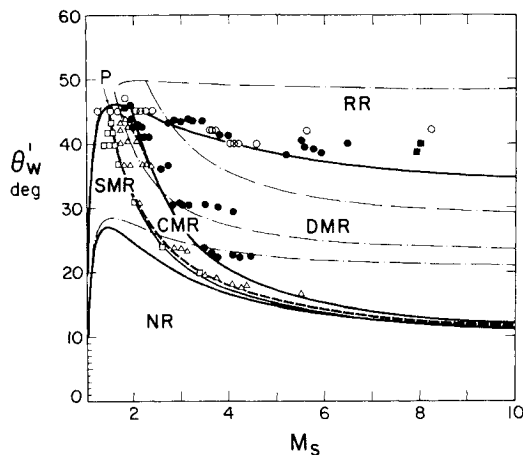


Fig. 9a   Regions and transition lines of regular (RR) and Mach (MR) reflections in the $(M_s,\theta_w)$ plane for vibrational equilibrium SF$_6$ and experimental data. For SMR$\leftrightarrow$CMR transition boundary, solid line represents $M_{2T} = 1$ and dashed line represents $\delta = 90$ deg. Dash-dot lines are for frozen SF$_6$ $(\gamma = 4/3)$. Experimental data: ■ TDMR, ○ RR, □ SMR, △ CMR, ● DMR (Ref. 38).



Fig. 9c   Regions and transition lines of regular (RR) and Mach (MR) reflections in the $(M_s,\theta_w)$ plane for SF$_6$ as a perfect gas $(\gamma = 1.093)$ and experimental data. For SMR$\leftrightarrow$CMR transition boundary, solid line represents $M_{2T} = 1$ and dashed line represents $\delta = 90$ deg. Experimental data: ■ TDMR, ○ RR, □ SMR, △ CMR, ● DMR (Ref. 38).



Fig. 9b   Regions and transition lines of regular (RR) and Mach (MR) reflections in the $(M_s,\theta_w')$ plane for vibrational equilibrium SF$_6$ and experimental data. For SMR$\leftrightarrow$CMR transition boundary, solid line represents $M_{2T} = 1$ and dashed line represents $\delta = 90$ deg. Dash-dot lines are for frozen SF$_6$ $(\gamma = 4/3)$. Experimental data: ■ TDMR, ○ RR, □ SMR, △ CMR, ● DMR (Ref. 38). NR is the no-reflection region.



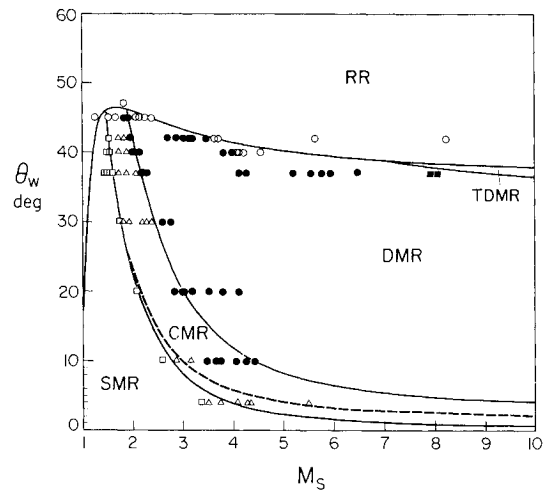Fig. 9d   Regions and transition lines of regular (RR) and Mach (MR) reflections in the $(M_s,\theta_w')$ plane for SF$_6$ as a perfect gas $(\gamma = 1.093)$ and experimental data. For SMR$\leftrightarrow$CMR transition boundary, solid line represents $M_{2T} = 1$ and dashed line represents $\delta = 90$ deg. Experimental data: ■ TDMR, ○ RR, □ SMR, △ CMR, ● DMR (Ref. 38). NR is the no-reflection region.
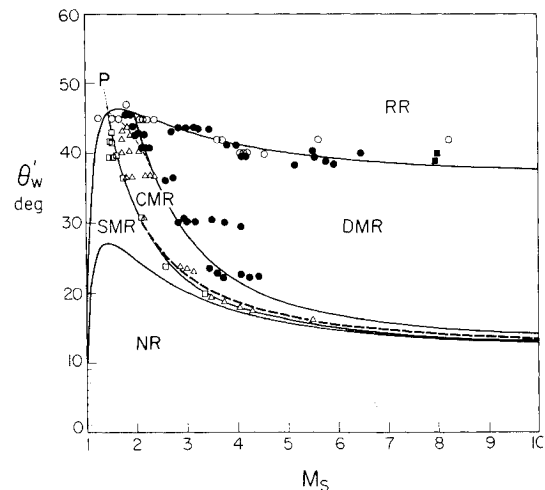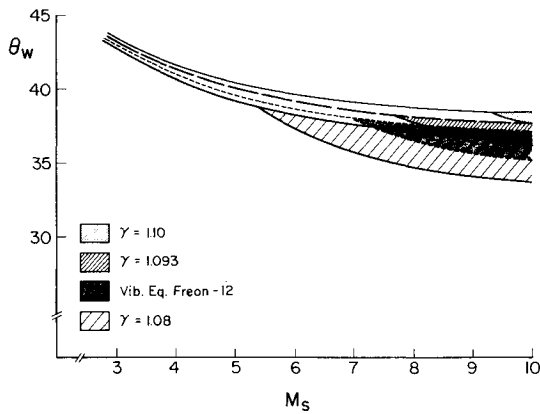
**Fig. 10a**   TDMR regions in $(M_s, \theta_w)$ plane for vibrational equilibrium Freon-12 and for perfect gases with $\gamma = 1.10$, 1.093, and 1.08.
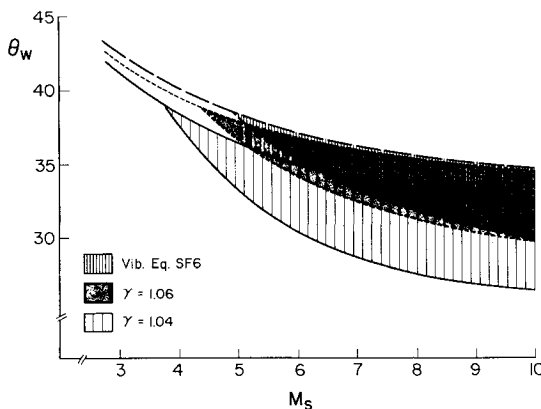


**Fig. 10b**   TDMR regions in $(M_s, \theta_w)$ plane for vibrational equilibrium $SF_6$, $\gamma = 1.06$, and $\gamma = 1.04$.
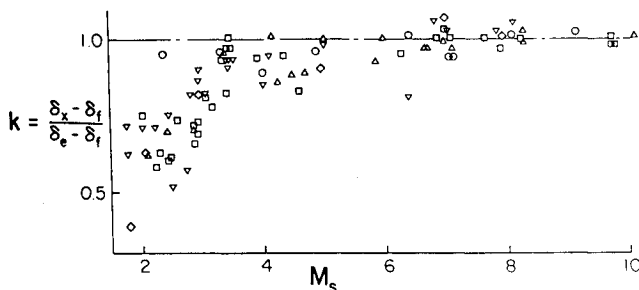


**Fig. 11**   Variation of departure of experimental $\delta_x$ from frozen-gas calculation $(\delta_x - \delta_f)$ normalized by the difference between equilibrium- and frozen-gas calculations $(\delta_e - \delta_f)$ (Ref. 43).
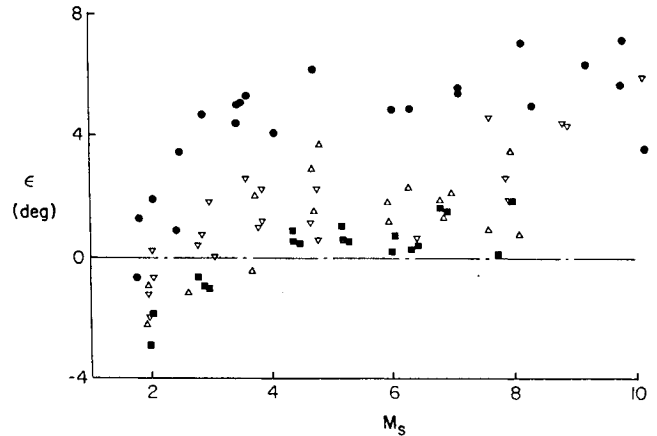


**Fig. 12**   Variation of experimental $\epsilon$ with incident shock-wave Mach number $M_s$ (Ref. 43): $\triangle$, $N_2$ (Ref. 30); $\blacksquare$, Ar (Ref. 30); $\bullet$, $CO_2$ (Ref. 37); $\triangledown$, air (Ref. 36).
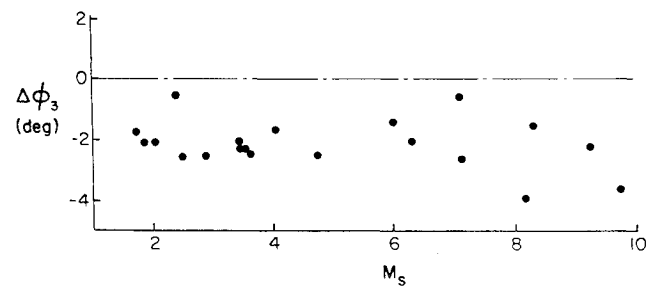


**Fig. 13**   Difference in the incident wave angle to the Mach stem $\Delta\phi_3$ between experimental and numerical results for $CO_2$ (Ref. 43): Experimental results from Ref. 37.

transition line in the CMR region and four below in the DMR regime at $M_s \sim 2$, and four below at $M_s \sim 4$, showing a persistence of RR. Several DMR runs lie in the CMR region at $\theta_w \sim$ 45, 43, 40, 20 deg, and especially at 10 deg. All CMR runs lie properly in their region at or below the $M_{2T} = 1$ line, except two in the SMR region at $M_s \sim 3.5$. The equilibrium plot of Fig. 9a is superior since the RR→MR line lies lower for lower $\gamma$ than for the fixed ($\gamma = 1.093$) line of Fig. 9c. The SMR→CMR and CMR→DMR lines are also better in Fig. 9a for the same reason, providing better agreement with experiment overall for the equilibrium plot.

Figure 9d provides the $(M_s, \theta'_w)$ plot for $\gamma = 1.093$. For overall agreement, it is not as good as Fig. 9b. Here three DMR's lie in the CMR region at $M_s \sim 3.5$ and several at $M_s \sim 2$. These would lie correctly in the DMR region if the CMR→DMR line were curved to join the SMR→CMR line to

the RR→MR line at point P, as noted previously. On the other hand, several DMR's and the two TDMR's lie in the RR region. Overall, the equilibrium curves of Fig. 9b provide better agreement.

Figure 10a shows the extent of the TDMR over a range of $\gamma$ as well as for vibrational equilibrium Freon-12 and $SF_6$. It is seen that the regions are bounded by the two-shock theory RR↔MR transition line and the line along which $\chi' = 0$. The region for a perfect gas with $\gamma = 1.10$ is very small, and occurs for $M_s > 9$ and $\theta_w \sim 38$ deg. For a perfect gas with $\gamma = 1.093$, the region is much larger and occurs for $M_s > 7.5$ and $\theta_w > 37$ deg. For vibrational equilibrium Freon-12, the region is much larger still and starts at $M_s \sim 7$. For $\gamma = 1.08$, the TDMR region is quite large and starts at $M_s \sim 5$. Note that, unlike the results of Ikui et al. shown in Fig. 8a, the TDMR experiments are supposed to lie in the DMR region, not in the RR regime, as they found. It is not clear why this has happened. Even if the three-shock theory RR→MR line was used and $\chi'$ was in error by 1 or 2 deg, it would not account for this larger discrepancy, as can be seen from Fig. 10b. One can only speculate that the RR↔MR transition line is not appropriate for pseudostationary flows.

Figure 10b shows the regions of TDMR for vibrational equilibrium $SF_6$, $\gamma = 1.06$ and 1.04. It is seen that the regions become progressively larger. It should be possible to observe TDMR in vibrational equilibrium $SF_6$ at $M_s \sim 5$. Ikui et al.[25] observed TDMR in Freon-12 at $M_s \sim 3.8$ and $\theta_w \sim 46$ deg, and the present analysis shows this to occur at $M_s \sim 7$ and $\theta_w \sim 37$ deg. Consequently, this problem will require a resolution in the near future.

In summary, it can be stated that the $(M_s, \theta_w)$ plots provide the experimenter with good engineering results for all gases. Whether a point lies in one region or another sometimes depends on personal judgment when the result is not clear cut.

Consequently, it is more important to make measurements of the angles $\delta$, $\chi$, and $\omega'$, which are quantitative experimental results, and compare them with their counterparts from analysis using two- and three-shock theories, as applicable, in order to provide better tests for the state of the gas—frozen or equilibrium. The induced boundary layer causes $\delta$ to be larger and $\omega'$ to be smaller. Consequently, one can learn a good deal about the boundary layer itself from such measurements. The angle $\chi$ can be affected by the fact that the inclination of the slipstream $S$ depends on the two velocities on either side of the ideal contact surface, one in state (2) moving at a higher velocity than that in state (3). Consequently, the velocities in states (2) and (3) diverge due to the layer thickness, giving rise to a deflection, $\alpha$, which could affect $\chi$, as well as the relation $\theta_1 - \theta_2 = \theta_3$, used in the three-shock theory.

### Critique

It has been shown above that many experiments in various gases have now been performed on regular and Mach reflections of oblique shock waves in pseudostationary flow. The experimental agreement with the analytical boundaries for such reflections using two- and three-shock theories are reasonable but not precise enough over the entire range of incident shock-wave Mach numbers $(M_s)$ and compression wedge angle $(\theta_w)$. In order to improve the agreement, the assumptions and criteria employed in the analysis were critically examined using the foregoing experimental data.[43]

Several criteria were proposed to predict analytically the transition boundaries between the various reflections. However, the first complete transition solution in the $(m_s, \theta_w)$ or $(M_s, \theta_w')$ plane using two- and three-shock theories and the relevant criteria to obtain the transition lines were given in Refs. 30 and 31, respectively, for $N_2$ and Ar; in Ref. 37 for $CO_2$; in Ref. 28 for perfect and equilibrium air up to $M_s = 20$; in Ref. 38 for $SF_6$; and in the present paper for Freon-12.[25]

### Comparison of Experimental and Numerical Values of $\delta$

It has been noted previously that by measuring the angles $\delta$, $\chi$, and $\omega'$, it is possible to obtain quantitative checks with analysis as well as inferring the state of the gas, whether it was frozen or in equilibrium. A minimum finite length of 1 mm is required to measure the slope of a shock wave from an interferogram. The measured angle is then the average slope within this length. The vibrational relaxation length $\ell_v$ at $P_0 = 15$ Torr and $T_0 = 300$ K becomes[55] 1 mm at $M_s \sim 8$ for $O_2$, $M_s > 10$ for $N_2$, $M_s \sim 5$ for $CO_2$, and $M_s \sim 2$ for $SF_6$. In two and three shock-wave systems for regular and Mach reflections, the relaxation lengths do not vary significantly[43] com-

pared to a $10^2$-$10^7$ variation in $\ell_v$ for $2 < M_s < 10$. Consequently, the Mach number at which $\ell_v = 1$ mm behind each shock wave in Mach reflection does not differ very much. Therefore, the choice of 1 mm as a characteristic flow length is quite reasonable. When the relaxation length is of the same order as the characteristic length, the simplified two- and three-shock theories can no longer be used. Therefore, it is reasonable to apply a frozen $(\ell_v \gg 1$ mm) flow or an equilibrium $(\ell_v \ll 1$ mm) flow assumption. Only vibrational excitation need be considered in the present experiments as dissociation, electronic excitation, and ionization relaxation lengths are much longer than 1 mm in the present shock Mach number and pressure ranges of the experiments. Air with 21% $O_2$ is an exception at high shock Mach numbers. However, dissociation is negligible for $M_s < 10$. The specific heat ratio for frozen-gas calculation is 5/3 for Ar; 7/5 for $N_2$, $O_2$, air, and $CO_2$ (linear molecule); and 4/3 for Freon-12 and $SF_6$.

In Ref. 43, there are several plots of the variation of angle $\delta$, with shock Mach number for fixed effective wedge angle $\theta_w'$ for $CO_2$, $N_2$, and Ar, and in Ref. 38 for $SF_6$. These may be condensed by plotting the quantity $k = (\delta_x - \delta_f)/(\delta_e - \delta_f)$ where $\delta_x$ is the measured $\delta$, $\delta_f$ the calculated frozen $\delta$, and $\delta_e$ the calculated equilibrium $\delta$. It is seen from Fig. 11 for $CO_2$, for example, that for $M_s > 4$, $k \rightarrow 1$; i.e., $\delta_x = \delta_e$ and the agreement is for $CO_2$ in equilibrium, despite the fact that the experiments in the $(M_s, \theta_w)$ plane agree best with a perfect gas $(\gamma = 1.29)$. These results are more reliable: As no transition criteria are required in the calculation of $\delta$, a quantitative comparison can be made for each pair of analytical and experimental points; a measurement of $\delta$ has no ambiguity unlike the classification of the reflection types near the transition boundaries where, for example, a CMR may look like an SMR or a CMR like a DMR. The parameter $\theta_w'$ should be used instead of $\theta_w$ in the comparisons, since $\theta_w'$ can be obtained directly from Eqs. (1-4), while $\theta_w$ is derived by assuming that the Mach stem $M$ is perpendicular to the wedge surface at the triple point. This is not always the case experimentally, as shown subsequently.

### Effects of Mach Stem Curvature

In Figs. 1 and 2, all of the Mach stems $M$ are drawn ideally perpendicular to the wedge surface from the triple point T. In reality, the Mach stem can have a convex curvature $(+)$ at an angle $\epsilon$ from T or with a concave $(-)$ curvature but again ending up perpendicular to the wedge surface.



a) **Interferogram and experimental isopycnics region and $\rho/\rho_0$. (0) 1.00; (1) 2.71; (2) 3.68; (3) 3.33; (a) 3.36; (b) 3.44; (c) 3.52; (d) 3.60; (e) 3.68; (f) 3.75; (g) 3.83; (h) 3.91; (i) 3.99; (j) 4.06; (k) 4.14.**



Fig. 14 Comparison of experimental reflected wave angle $\omega'$ with numerical results for various displacement angles $\theta_d$ for $CO_2$: Experimental points (Ref. 37): $\triangledown, \theta_w = 45.5$ deg; $\square$, $\theta_w = 47$ deg; $\circ, \theta_w = 50$ deg; $\triangle, \theta_w = 60$ deg; lines (equilibrium-gas calculation): ———, $\theta_d = 0$ deg; ———, $\theta_d = -1$ deg; ---, $\theta_d = -2$ deg (Ref. 43).
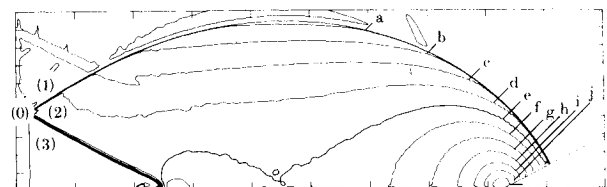
b) **Numerically simulated isopycnics by Glaz et al.[34] shown in Fig. 15a.**

Fig. 15 SMR, $M_s = 2.03$, $\theta_w = 27$ deg, $p_0 = 33.3$ kPa, $T_0 = 299.2$ K. Air, $\rho_0 = 0.387$ kg/m$^3$.

The Mach stem was assumed perpendicular to the wedge surface at the triple point in deriving $\theta_w$ from $\phi_3$ in the three-shock theory. The deviation $\epsilon$ from this idealization is shown for Ar, $N_2$, air, and $CO_2$ in Fig. 12. It is seen that $\epsilon$ has positive values (0–8 deg) for $M_s > 4$ and decreases to negative values ($-3$ deg) at $M_s = 2$. Consequently, $\theta_w$ as derived from $\phi_3$ has an error equal to $\epsilon$. Therefore, comparisons of quantities in Mach reflection should be made with $\theta_w'$, as long as $\epsilon$ cannot be predicted accurately. This error is the main reason for the inaccurate prediction of $\chi$ using the three-shock theory.

In Fig. 13, the effect of $\epsilon$ on $\phi_3$ is shown for $CO_2$ as the variation of $\Delta\phi_3 = \phi_3$ (numerical) $- \phi_3$ (experimental) with shock Mach number $M_s$. The numerical results are based on an equilibrium gas, verified in Fig. 11. It is seen that $\Delta\phi_3$ has a value of about $-2$ deg, independent of $M_s$. The results for other gases are similar albeit somewhat more dispersed.

### Effect of Slipstream Thickness

In the solution of Eqs. (1–4), only the pressures [Eq. (7)] and flow directions [Eq. (8)] were assumed to be continuous across the slipstream, an idealized surface. In reality, it is a shear layer of increasing finite thickness, where the velocity in state (2) is greater than that in state (3) and the temperature in state (3) is greater than that in state (2). Near the triple point the layers are laminar; beyond they become turbulent. Consequently, as noted previously, the shear-layer thickness gives rise to a deflection of the velocities in states (2) and (3). If it is assumed that the velocity displacement in the layer $\alpha$ exists at the triple point, then its possible affect on $\chi$ should be taken into account in the discrepancies between the numerical and experimental values of $\chi$.

### Effect of Shock-Induced Boundary-Layer on the Wedge Surface

It has been found by many experimenters that RR persists into the MR regime. This has been called the "von Neumann paradox." Recently, several analyses[39,43,45] have shown that this is due to the boundary-layer negative displacement thickness. Consequently, the displaced wall is below the actual wall. The reflected wave $R$ moves below to a new position so that the angle $\delta$ between $I$ and $R$ is now larger or the reflected wave angle $\omega'$ is smaller.[55] The condition $\theta_1 - \theta_2 = \theta_d$ must now be used instead of Eq. (6). This can be checked and has been verified experimentally. Figure 14 compares experimental $\omega'$ for $CO_2$ with calculations for several values of $\theta_d$. The experimental results lie between the lines of $\theta_d = 0$ and $-2$ deg. Similar results were obtained for Ar, $N_2$, and air. A displacement angle $\theta_d = -1$ deg shifts the RR↔MR von Neumann detachment transition boundary by $\Delta\theta_w = -0.7$ deg for $N_2$ and air, and $\Delta\theta_w = -0.5$ for $CO_2$. Recently, Sakurai[46] proposed to use a pseudostationary RR↔MR criterion. However, its effectiveness is yet to be tested experimentally.

## Flowfield Solutions

The foregoing dealt with simplified algebraic solutions[48] for RR and MR, which involved mainly the shock waves and the slipstream. In order to compare experimental and analytical solutions of the entire flowfield for such sensitive parameters as the density distribution, which can be measured interferometrically, it is necessary to solve the time-dependent[33,34] or pseudostationary Euler equations as noted subsequently, for a perfect or equilibrium gas. Otherwise, it would be necessary to use rate equations for equilibration as well.

Continuity:

$$\rho_t + (\rho u)_x + (\rho v)_y = 0$$

Momentum:

$$(\rho u)_t + (\rho u^2 + p)_x + (\rho u v)_y = 0$$
$$(\rho v)_t + (\rho v)_x + (\rho v^2 + p)_y = 0 \tag{9}$$

Energy:

$$(\rho E)_t + (\rho u E + u p)_x + (\rho v E + v p)_y = 0$$

where $\rho$ is the density, $u = (u, v)$ is the velocity field, $E = \frac{1}{2}(u^2 + v^2) + e$ is the total specific energy, $e$ is the specific internal energy, and $p$ is the pressure. The system is closed by specifying an equation of state (EOS).

$$p = p(\rho, e) \tag{10}$$

Such an equation can be obtained from the thermal equation of state $p = \rho R T$ and the specific internal energy for a perfect gas $e = C_v T$, to yield

$$p = (\gamma - 1)\rho e \tag{11}$$

where $\gamma > 1$ is the ratio of specific heats and is considered to be a constant. For gases such as $CO_2$ and $SF_6$ in vibrational equilibrium the equation of state has to be modified. For self-similar motion, the problem has no intrinsic length scale. Consequently, a new pseudostationary coordinate system can be used, such that $(\xi, \eta) = [(x - x_0)/(t - t_0), (y - y_0)/(t - t_0)]$, where $(x_0, y_0)$ are the coordinates of the wedge corner $C$, and $t_0$ is the time when the incident shock wave $I$ reaches the corner. As shown by Jones et al.,[23] the system of Eq. (9) can be transformed into a pseudostationary system [Eq. (12)].[34]

$$(\rho\tilde{u})_\xi + (\rho\tilde{v})_\eta = -2\rho$$

$$(\rho\tilde{u}^2 + p)_\xi + (\rho\tilde{u}\tilde{v})_\eta = -3\rho\tilde{u}$$

$$(\rho\tilde{u}\tilde{v})_\xi + (\rho\tilde{v}^2 + p)_\eta = -3\rho\tilde{v}$$

$$(\rho\tilde{u}\tilde{H})_\xi + (\rho\tilde{v}\tilde{H})_\eta = -\rho(\tilde{u}^2 + \tilde{v}^2) - 2\rho\tilde{H} \tag{12}$$

where

$$\tilde{u} = u - \xi, \qquad \tilde{v} = v - \eta, \qquad \tilde{H} = \frac{1}{2}(\tilde{u}^2 + \tilde{v}^2) + h \tag{13}$$

and $h = e + p/\rho$ is the specific enthalpy. Also $(\tilde{u}, \tilde{v})$ and $\tilde{H}$ are referred to as the self-similar velocity field and self-similar total enthalpy, respectively. In addition $\tilde{M}$ is defined by

$$\tilde{M}^2 = (\tilde{u}^2 + \tilde{v}^2)/a^2 \tag{14}$$

where $a$ is the sound speed and $\tilde{M}$ is called the self-similar Mach number. The system of Eq. (12) is the steady Euler equations with the addition of source terms. Note that the ratio $s/L$ is constant (Fig. 1c) for given initial conditions, for self-similar solutions of the nonstationary equations just as $s$ is contant for steady supersonic flow. In this and other ways, a change to pseudostationary coordinates is very useful in the analysis of such flowfields and was used in numerical simulations of the interferometric experiments on oblique shock-wave reflections.[33]

Perhaps the best example of showing the great strides that have taken place in the reliability of numerical simulation of such problems is to compare the results of Schneyer,[47] of a decade ago, with the present state-of-the-art simulation by Glaz et al.[34] Figure 15a shows an interferogram of an SMR in air at $M_s = 2.03$, $\theta_w = 27$ deg, $p_0 = 250$ Torr, and $T_0 = 300$ K. The lines of constant density (isopycnics) over the flowfield are also shown in the caption. Figure 15b shows the same case treated by Glaz et al.[34] a decade later, which is a very good simulation indeed. Many such cases were treated in air, Ar, and $SF_6$.[34,35,49] The agreements with experiments are all surprisingly good considering that the simulations utilized the Euler equations for inviscid flow and the interferograms are for real flows with viscosity and real-gas effects. Needless to say, the simulations provide numerous data on pressure, temperature, Mach number, enthalpy, etc., that cannot readily be

| Region | $\rho/\rho_0$ |
|--------|---------------|
| 0 | 1.00 |
| 1 | 8.47 |
| 2 | 10.33 |
| 3 | 9.12 |
| a | 8.47 |
| b | 7.18 |
| c | 5.89 |
| d | 9.76 |
| e | 11.04 |
| f | 12.31 |
| g | 13.58 |
| h | 14.86 |
| i | 16.13 |
| j | 17.41 |
| k | 18.68 |
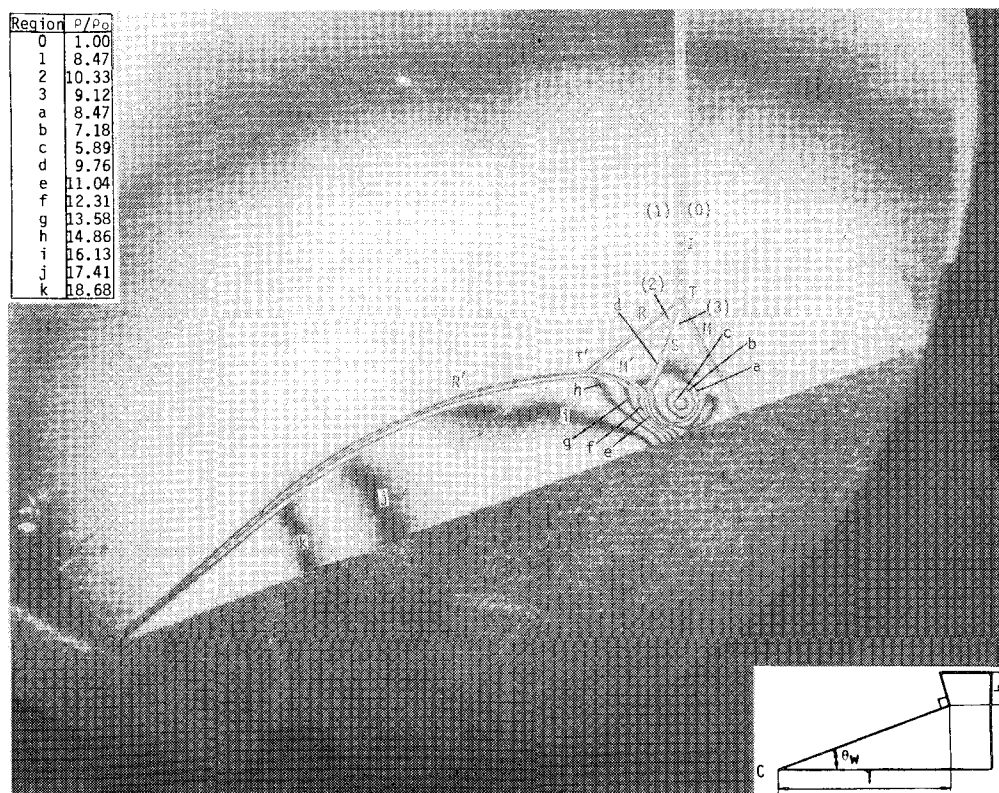
Fig. 16a    Collision of DMR with a 90-deg ramp in $CO_2$, $\theta_w = 20$ deg, $\ell = 134$ mm, $h = 12.7$ mm, $P_0 = 10$ Torr, $\lambda = 6943$ Å. An interferogram taken at $t = 59$ $\mu$s, $M_s = 5.81$, $T_0 = 297$ K, and $\rho_0 = 2.38 \times 10^{-5}$ g/cm$^3$. $\Delta\rho/\rho_0 = 1.27$. $I$, incident shock wave; $M$, first Mach stem; $M'$, second Mach stem; $R$, first reflected shock wave; $R'$, second reflected shock wave; $T$, first triple point; $T'$ second triple point (Ref. 24).



| Region | $\rho/\rho_0$ | Region | $\rho/\rho_0$ |
|--------|---------------|--------|---------------|
| 0 | 1.00 | o | 25.43 |
| 1 | 8.43 | p | 27.96 |
| 2 | 10.29 | q | 30.48 |
| 3 | 9.09 | r | 33.00 |
| a | 2.72 | s | 40.58 |
| b | 3.98 | t | 48.15 |
| c | 5.24 | u | 55.72 |
| d | 5.24 | v | 63.29 |
| e | 6.50 | w | 70.86 |
| f | 7.76 | x | 73.39 |
| g | 9.03 | y | 75.91 |
| h | 10.29 | | |
| i | 11.55 | | |
| j | 12.81 | | |
| k | 15.34 | | |
| l | 17.86 | | |
| m | 20.38 | | |
| n | 22.91 | | |

Fig. 16b    An interferogram taken at $t = 119$ $\mu$s, $M_s = 5.78$, $T_0 = 294$ K, $\rho_0 = 2.40 \times 10^{-5}$ g/cm$^3$, $\Delta\rho/\rho_0 = 1.26$. $B$, bifurcation of shock wave; $C_1$, contact front; $E$, expansion wave; $I$, incident shock wave; $P$, protrusion due to local sidewall boundary-layer separation; $S_1$ to $S_7$, shock waves; $R$, rarefaction wave.

Fig. 17a  Numerical simulation of the collision of a DMR with a 90-deg ramp in $CO_2$. Thirty equally spaced numerical isopycnics. Conditions as for Fig. 16a. Note that the interaction of the Mach stem with the rolled-up slipstream is more severe than in the interferogram. In addition, a second triple-point system and slipstream appear at the kink in the Mach stem. A second normal shock wave, to the left of the curved Mach stem, separated by a contact surface, can also be seen. These transitions do not appear in the interferogram and are suppressed by the induced boundary layer. (See Refs. 33 and 34 for similar results in air, etc.).



Figs. 17b  Numerical simulation of the collision of a DMR with a 90-deg ramp in $CO_2$. Thirty equally spaced numerical isopycnics. Conditions as for Fig. 16b. The inviscid results are modeled quite well except for the position of contact surface $C_1$ and the recompression shock wave $S_7$. However, the viscous effects, such as the shock-wave bifurcation $B$ and the protrusion $P$, due to the local boundary-layer separation on the window, are not modeled, as expected. This effectively points out the necessity of redoing such simulations using the Navier-Stokes equations.

measured experimentally. Undoubtedly, repeat simulations using the Navier-Stokes equations and equilibration rate equations for the degrees of excitation involved would provide some important answers as to whether the costly refinements were warranted.

It is worth noting that some very worthwhile concepts have been added to pseudostationary oblique shock-wave reflections recently, using the Monte-Carlo technique. Here the reflections are simulated at the molecular level by using a large number of particle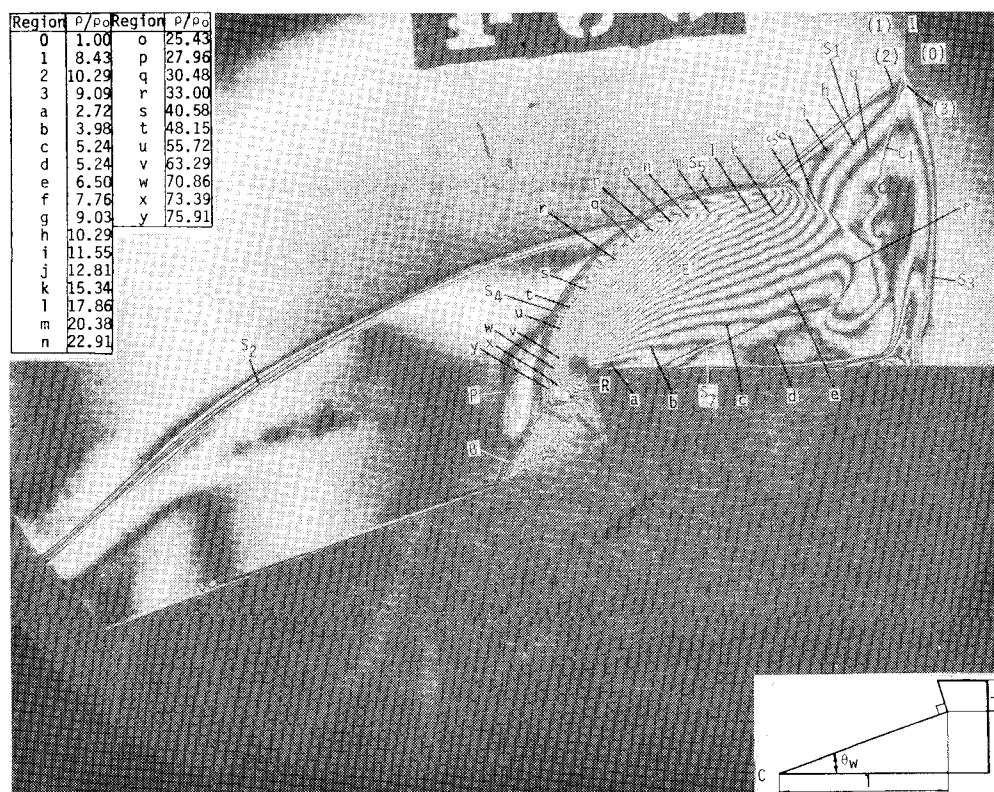s ($> 10,000$) and following their positions in phase space.[50,51] Of the two papers, Seiler's paper[51] is of greater interest since he treated both specular and diffuse reflections of the hard-sphere molecules and, therefore, was able to obtain the boundary layer induced by the incident and reflected shock waves in RR at the reflection point. Seiler's results confirm that RR persists into the MR regimes as a result of the induced boundary layer. He also showed that the reflected wave angle $\omega'$ is smaller as a result. However, the method will have to be refined to produce sharper shock waves, well-defined slipstreams, and more meaningful isolines compared with experimental interferograms and the numerical simulations obtained by Glaz et al.[33-35,49] Unfortunately, Seiler did not investigate the expansion-compression wave-system model produced by the boundary-layer displacement thickness

at its leading edge, used by several investigators in order to substantiate if at the molecular level the model is correct, since it cannot be seen in optical enlargements of the flow.

A more complex simulation is that of a problem where self-similarity cannot be applied. For example, the collision of a Mach reflection with a 90-deg ramp on the wedge surface provides such a case.[24,49] Figure 16a shows an interferogram of a DMR in $CO_2$, $M_s = 5.81$, $\theta_w = 20$ deg, $p_0 = 10$ Torr, $T_0 = 297$ K before colliding with a 12.7-mm ramp. Figure 16b shows the wave system 60 $\mu$s later, after the collision had taken place. It is seen that the wave system involving Mach stem-slipstream interactions, boundary-layer interactions, rarefaction, and expansion waves, etc., has become very complex. The type of interaction is dependent on the relative heights of Mach stem and ramp. Figure 17 shows the numerical simulations. Surprisingly good agreement is obtained of the main features of the flow using the Euler equations of motion. However, the viscous effects are not simulated and effectively show the need for using the Navier-Stokes equations for adequate simulation. Many additional details can be found in Refs. 24 and 49.

## Conclusions

1) Although much has been learned about oblique shock-wave reflections since Mach[22] wrote his pioneering paper in 1878, a great deal is still to be known. The best available data to date from several sources on such reflections have been presented graphically in an consistent format.

2) The presently accepted transition lines for RR↔MR, SMR↔CMR, and CMR↔DMR provide very reasonable engineering answers as to the type of reflection that will occur, given $M_s, \theta_w$, and $\gamma$ for frozen and perfect gases and for vibrational equilibrium given additionally $T_0$. For gases with low $\gamma$ at room temperature, such as $CO_2$, Freon-12, and $SF_6$, real-gas effects in vibration are very important and must be taken into account. They are not precise enough, and improved transition-line criteria will have to be found to account for those experiments that give rise to the "von Neumann paradox" for the RR↔MR transition. For the SMR↔CMR and CMR↔DMR lines at lower $\theta_w$, where a number of experiments fall outside the present lines (see Figs. 7-9), new criteria will have to remedy this situation.

3) The experimental CMR↔DMR line leading to point P on the RR↔MR line will have to be replaced by an analytical line (see Figs. 9a, 9b, and 9d).

4) It is not clear whether the induced boundary-layer slope or thickness is the important parameter to account for the "von Neumann paradox." Some experiments with induced turbulent boundary layers caused by specified roughness should help in a decision on this point.

5) It is not known why the TDMR experiments lie in the RR regime rather than in the DMR region as predicted from the condition $\chi' = 0$. Perhaps the von Neumann RR→MR line is not applicable to pseudostationary flow.

6) More needs to be known about RR and MR over rough surfaces, spongy surfaces, surfaces with a thin layer of He or other gases, and in a dusty-air environment.

7) Improved computational simulations using the Navier-Stokes equations and real-gas rate equations are required for a comparison with the available interferometric data.

It can be seen that much work still remains to be done in pseudostationary oblique shock-wave reflections in order to answer some of the above-noted problems. Undoubtedly, such work will be forthcoming in the near future. In addition to the single-wedge problems, the degree of complexity increases using multiple straight wedges, as well as convex and concave wedges.[53,54] For further details see Ref. 55.

## Acknowledgments

It is a pleasure to acknowledge the fine research conducted over the years on pseudostationary oblique shock-wave reflections by my former master's and Ph.D. candidates: R. R.

## References

[1]Glass, I. I. "Shock Waves and Man," published by UTIAS, printed by University of Toronto Press, Canada, 1974.

[2]Glass, I. I., "Shock Waves on Earth and in Space," *Progress in Aerospace Sciences*, 1977, pp. 279-286.

[3]Glass, I. I., "Terrestrial and Cosmic Shock Waves," *American Scientist*, Vol. 65, No. 4, 1977, pp. 473-481.

[4]Fowler, R. G., "Lightning," *Applied Atomic Physics*, Vol. 5, Academic Press, New York, 1982, pp. 31-67.

[5]Ribner, H. S. and Roy, D., "Acoustics of Thunder: A Quasilinear Model for Tortuous Lightning," *Journal of the Acoustical Society of America*, Vol. 72, No. 6, 1982, pp. 1911-1925.

[6]Rable, R. G., "Earth's Global Electrical Circuit: An Unsolved Mystery," *Aerospace America*, Jan. 1985, pp. 124-127.

[7]Hubert, P., "Triggered Lightning in France and New Mexico," *Endeavor*, Vol. 8, No. 2, 1984, pp. 85-89.

[8]Bar Nun, A., "Shock Waves and the Origin of Life," UTIAS Review No. 41, 1976.

[9]Glasstone, S., "Effects of Nuclear Weapons," U. S. Government Printing Office, Washington, D.C., 1962; also Brode, H. L., "Air Blast from Nuclear Bursts," Pacific-Serra Research Corp., Santa Monica, CA, Rept. 1419-1, 1984.

[10]"The Final Chapter?," TV Ontario Program, Nov. 19, 1985.

[11]Lerner, E. I., "Star Wars: Feasibility Key to Policy Debate," *Aerospace America*, Aug. 1985, pp. 39-42.

[12]Glass, I. I. and Hall, J. G., *Handbook of Supersonic Aerodynamics*, Sec. 18, "Shock Tubes," U.S. Government Printing Office, Washington, D.C., 1959.

[13]Baker, W. E., *Explosions in Air*, University of Texas Press, Austin, TX, 1973.

[14]Liepmann, H. W. and Roshko, A., *Elements of Gasdynamics*, Wiley, London, 1957.

[15]"The Mountain That Roared," *National Geographic*, Vol. 159, No. 1, 1981, pp. 54-55.

[16]Kerr, R. A., "When Disaster Rains Down from the Sky," *Science*, 206, Nov. 10, 1979, pp. 803-804; see also Weaver, K. F., "Meteorites—Invaders from Space," *National Geographic*, Sept. 1986, pp. 291-418.

[17]Brochure on the Dornier Kidney Lithotripter, Dornier Medical Systems, Marietta, GA, 1985; also, Potter, E., President, Dornier Medical Systems, private communication.

[18]Kambe, K., et al., "Underwater Shock-Wave Focusing—An Application to Extracorporeal Lithotripsy," *Proceedings of the 15th International Symposium on Shock Waves and Shock Tubes*, Berkeley, CA, 1985, pp. 641-647; also Watanabe, H., Shiino, K., and Oinuma, S., "Micro-Explosion Cystolithotrip," *Japanese Journal of Urology*, 1983, Vol. 129, pp. 23-28.

[19]Russell, D., "Shock Dynamics of Noninvasive Fracturing of Kidney Stones," *Proceedings of the 15th International Symposium on Shock Waves and Shock Tubes*, Berkeley, CA, 1985, pp. 57-64.

[20]Shima, E., Matsuda, T., Takeda, H., and Sawada, K., "Hydrodynamic Calculations of Axisymmetric Accreton Flow,"

Dept. of Aero. Eng., Kyoto University, Japan, Rept. KVCD 85-1, 1985.

[21]Hu, W-R., "A Gaseous Shock Wave Theory of the Galactic Spiral Structure," *Applied Mathematics and Mechanics*, Vol. 3, No. 2, April 1982, (English Edition), pp. 195-216.

[22]Mach, E., "Uber den Vevlauf des Funkenwellen in der Ebene und in Raume," Oesterreichische Akademie der Wissenschaften, Matematischnaturwissenschaftliche Klasse, Sitzungsbechichrte Abt. II, Vol. 78, 1878, pp. 819-838.

[23]Jones, D. H., Martin, P. M. E., and Thornhill, C. K., "A Note on the Pseudo-Stationary Flow Behind a Strong Shock Diffracted or Reflected at a Corner," *Proceedings of the Royal Society, London*, Ser. A, Vol. 4208, 1951, p. 238.

[24]Li, J-C. and Glass, I. I., "Collision of Mach Reflections with a 90-Degree Ramp in Air and $CO_2$," UTIAS Rept. 290, 1985.

[25]Ikui, T., Matsuo, K., Aoki, T., and Kondoh, N., "Mach Reflection of a Shock Wave from an Inclined Wall," *Memoirs, Faculty of Engineering, Kyushu University*, Vol. 41, No. 4, 1981, pp. 361-370.

[26]von Neumann, J., "Oblique Reflection of Shocks," Navy Dept., Bureau of Ordnance, Washington, D.C., Explosive Research Rept. 12, 1943.

[27]von Neumann, J., "Refraction, Intersection, and Reflection of Shock Waves," Navy Dept., Bureau of Ordnance, Washington, D.C., NAVORD Rept. 203-45, 1945.

[28]Lee, J-H. and Glass, I. I., "Pseudo-Stationary Oblique Shock-Wave Reflections in Frozen and Equilibrium Air," *Progress in Aerospace Sciences*, Vol. 21, No. 1, 1984, pp. 33-80.

[29]White, D. R., "An Experimental Survey of the Mach Reflection of Shock Waves," Dept. of Physics, Princeton University, Princeton, NJ, 1951, Tech. Rept. 11-10.

[30]Ben-Dor, G. and Glass, I.I., "Domains and Boundaries of Non-Stationary Oblique Shock-Wave Reflexions. 1. Diatomic Gas," *Journal of Fluid Mechanics*, Vol. 92, Pt. 3, 1979, pp. 459-496.

[31]Ben-Dor, G. and Glass, I. I., "Domains and Boundaries of Non-Stationary Oblique Shock-Wave Reflexions. 2. Monatomic Gas," *Journal of Fluid Mechanics*, Vol. 96, Pt. 4, 1980, pp. 735-756.

[32]Ben-Dor, G. and Glass, I. I., "Nonstationary Oblique Shock-Wave Reflections: Actual Isopycnics and Numerical Experiments," *AIAA Journal*, Vol. 16, Nov. 1978, pp. 1146-1153.

[33]Glaz, H. M., Colella, P., Glass, I. I., and Deschambault, R. L., "A Numerical, Graphical and Experimental Study of Oblique-Shock-Wave Reflections," Univeristy of Toronto Institute for Aerospace Studies, Canada, UTIAS, Rept. 285, 1986.

[34]Glaz, H. M., Colella, P., Glass, I. I., and Deschambault, R. L., "A Numerical Study of Oblique Shock-Wave Reflections with Experimental Comparisons," *Proceedings of the Royal Society, London*, Ser. A, Vol. 37, 1985, pp. 295-309.

[35]Glaz, H. M., Glass, I. I., Hu, T. C. J., and Walter, P. A., "Oblique Shock Wave Reflections in $SF_6$: A Comparison of Calculations and Experiment," *Dynamics of Explosions, Progress in Astronautics and Aeronautics*, edited by J.R. Bowen, J.-C. Leger, and R.I. Soloukhin, AIAA, New York, Vol. 106, pp. 359-387.

[36]Deschambault, R. L. and Glass, I. I., "An Update on Non-Stationary Oblique Shock-Wave Reflections: Actual Isopycnics and Numerical Experiments," *Journal of Fluid Mechanics*, Vol. 131, 1983, pp. 27-57.

[37]Ando, S. and Glass, I. I., "Domains and Boundaries of Pseudostationary Oblique-Shock-Wave Reflections in Carbon Dioxide," *Proceedings of the Seventh International Symposium on Military Applications of Blast Simulation*, Medicine Hat, Alberta, Canada, July 1981.

[38]Hu, T. C. J. and Glass, I. I., "An Interferometric and Numerical Study of Pseudo-Stationary Oblique-Shock-Wave Reflections in Sulfur Hexafluoride ($SF_6$)," *Proceedings of the 15th International Symposium on Shock Waves and Shock Tubes*, Berkeley, CA, July 1985, pp. 227-234.

[39]Wheeler, J., "An Interferometric Investigation of the Regular to Mach Reflection Transition Boundary in Pseudostationary Flow in Air," UTIAS Tech. Note 256, 1986.

[40]Mirels, H., "Mach Reflection Flowfields Associated with Strong Shocks," *AIAA Journal*, Vol. 23, April 1985.

[41]Law, C. K. and Glass, I. I., "Diffraction of Strong Shock Waves by a Sharp Compressive Corner," *CASI Transactions*, Vol. 4, 1971, pp. 2-12.

[42]Ben-Dor, G., "Analytical Solutions of Double-Mach Reflections," *AIAA Journal*, Vol. 18, 1980, p. 1036.

[43]Shirouzu, M. and Glass, I. I., "An Assessment of Recent Results on Pseudo-Stationary Oblique-Shock-Wave Reflections," University of Toronto Institute for Aerospace Studies, UTIAS Rept. 264, 1982; also, "Evaluation of Assumptions and Criteria in Pseudostationary

Oblique Shock-Wave Reflections," *Proceedings of the Royal Society, London*, 1986, pp. 75–92.

[44]Ben-Dor, G. and Takayama, K., "A Reconsideration of the Analytical Solution of a Pseudo-Steady Mach Reflection," to be published.

[45]Hornung, H. G. and Taylor, I. R., "Transition from Regular to Mach Reflection of Shock Waves," *Journal of Fluid Mechanics*, Vol. 123, 1982, pp. 143–153.

[46]Sakurai, A., "Modifications of the von Neumann Conditions for Weak Mach Reflection," presented at the 5th Mach Reflection Symposium, Stanford Research Institute, Menlo Park, CA, 1985.

[47]Schneyer, G. P., "Numerical Simulation of Regular and Mach Reflections," *The Physics of Fluids*, Vol. 18, No. 9, 1975, p. 1119.

[48]Hu, T. C. J. and Shirouzu, M., "Tabular and Graphical Solutions of Regular and Mach Reflections in Pseudo-Stationary Frozen and Vibrational-Equilibrium Flows," UTIAS Rept. 283, Pts. 1 and 2, Jan. 1985.

[49]Glaz, H. M., Glass, I. I., Li, J-C., and Walter, P. A., "Interaction of Oblique Shock-Wave Reflections in Air and $CO_2$ with Downstream Obstacles," *Proceedings of the 15th International Symposium on Shock Waves and Shock Tubes*, Berkeley, CA, July 1985, pp. 219–225.

[50]Meiburg, W., Oertel, H., Walenta, Z., Fiszdon, W., "Quasistationary Mach Reflection of Shock Waves, Preliminary Results of Experimental and Monte-Carlo Investigations," DFVLR-AVA Rept. IB 221-83A 15, 1983.

[51]Seiler, F., "Pseudo-Stationary Mach Reflection of Shock Waves," *Proceedings of the 15th International Symposium on Shock Waves and Shock Tubes*, Berkeley, CA, July 1985, pp. 129–138.

[52]Hu, T. C. J. and Glass, I. I., "Blast-Wave Trajectories from a Height-of-Burst," *AIAA Journal*, Vol. 24, April 1986, pp. 607–610.

[53]Ben-Dor, G., Takayama, K., and Kawauchi, T., "The Transition from Regular to Mach Reflexion and from Mach to Regular Reflexion in Truly Non-Stationary Flows," *Journal of Fluid Mechanics*, Vol. 100, Pt. 1, 1980, pp. 147–160.

[54]Dewey, J. M., Ben-Dor, G., and Takayama, K., "The Reflection of a Plane Shock Wave from a Double Wedge," presented at the 15th International Symposium on Shock Waves and Shock Tubes (15ISSWST), Berkeley, CA, 1985.

[55]Glass, I. I., "Some Aspects of Shock-Wave Research," AIAA Paper 86-0306, Jan. 1986.